PREDICITNG >10 MEV SEP EVENTS USING NEAR-RELATIVISTIC ELECTRON IN SITU PARTICLE DATA FROM ACE

by Katharine I. Kalamaroff

Space Radiation Laboratory

California Institute of Technology

2011

Glossary

CME - coronal mass ejection

Critical Event – any SEP event in which the integral 5-minute averaged intensity of greater than 10 MeV protons exceeds 30 pfu for at least 3 consecutive data points (15 minutes). The events considered in this study are "critical events".

Prediction Efficiency (of an alert) – percentage critical events that are accurately preceded by an alert

Event Onset Duration – Time (in minutes) over which proton intensity onsets from background and reaches 30 pfu.

False Alerts – Warnings of impending proton events that are not followed by a >10 MeV proton event which reaches 30 pfu within the next three hours.

Immediate Event – any critical event having an event onset duration less than two hours. These events often require more immediate operational responses.

Prediction Probability - probability that an alert will be followed by a >10 MeV proton event which reaches 30 pfu within the next three hours.

Proton Flux Units (pfu) – A measure of integral >10 MeV proton intensity: 1 pfu = 1 particle $cm^{-2}s^{-1}sr^{-1}$

SPE – solar particle event

SEP – solar energetic particle

Abstract

The sudden onsets of large solar energetic particle events threaten the operational ability of satellite and endanger personnel in space. Using *in situ* electron and proton intensity data from the ACE spacecraft, we have developed an algorithm which predicts the arrival of >10 MeV protons at Earth with 80% prediction efficiency. Three types of alerts are issued by this system: (1) magnetically well-connected alerts, (2) magnetically poorly-connected alerts, and (3) follow-on alerts. Each of these alerts have a prediction probability of 65%, 34%, and 25%, respectively, that they will be followed by an intensity of at least 30 pfu of >10 MeV protons within the next three hours. We discuss the simple algorithm used by this prediction system to issue these three types of alerts and analyze the reason for "false alerts".

1 Introduction

The Earth is continuously bathed in a shower of energetic particles of both solar and cosmic origin. While the terrestrial environment is somewhat protected from this barrage by the Earth's magnetic field, this incident radiation presents a regular hazard in the near-Earth space environment. Intense solar activity can lead to dramatic increases in the number of energetic particles from the Sun that reach Earth, elevating incident radiation five to six orders of magnitude on the timescale of minutes or hours (Mewaldt et al., 2007). These transient enhancements, known as solar particle events (SPEs), can have both acute and long-term impacts on electronic systems and humans in space. Roughly 96% of particle intensity incident on the Earth during SPEs is in the form of energetic protons. We are interested in predicting the onset of these energetic (greater than 10 MeV) protons, using purely *in situ* data, so that precautionary measures might be taken before their arrival.

1.1 Space Weather Hazards

The variability of radiation conditions in the near-Earth space environment is often referred to as "space weather", a term which includes both long-term modulation and short-term transience. Satellite engineers and mission planners can begin to account for known space weather hazards in the design phase, but the diverse effects energetic particles pose to both electronic and biological space systems make planning for all space weather hazards is a challenging task. To further mitigate the threats from SPES, space weather forecasting systems need to reliably predict their onset, minimizing false warnings and without missing radiation events (Kahler, Cliver, & Ling, 2007). The timescale over which forecasting is beneficial is

system dependent; a few minutes of lead time may allow for the safeguarding of satellites, but may be insufficient to protect astronauts in space.

1.1.1 Threats posed by SPEs to electronic systems

The type of threat posed by energetic particles to electronic systems in space varies with the energy and mass of the incident particles, so construction of a reliable forecasting scheme must be governed by the profiles of those particles deemed most threatening to a particular system. The National Oceanic and Atmospheric Administration - Space Weather Prediction Center (NOAA-SWPC) lists 6 types of spacecraft anomalies directly caused by solar energetic particles (Speich & Poppe, 2000): (1) surface charging, (2) deep dielectric or bulk charging, (3) single event upset (SEUs), (4) total dose effects, (5) photonics noise, and (6) materials degradation.

Degradation and spacecraft charging are extended effects resulting from long-term exposure to the space plasma environment. Degradation is defined as the erosion or deformation of satellite materials which may affect component performance. Spacecraft charging is defined as gradual collection of low energy (0.1 – 30 keV) electrons on the spacecraft, producing a differential electrostatic potential across the surface or internally. This buildup of charge may result in abrupt discharges that can affect satellite operation. These long-term effects may be accelerated by the large fluence of particles that arrive with SPEs.

Single event upsets, total dose effect, and photonics noise (increased device background), can result directly from SPEs experienced by the spacecraft. When energetic ions (greater than 50 MeV) penetrate shielding, they can strike sensitive electronics, causing bit-flipping and device tripping, the severity of which is highly dependent on incident location on the device. The

enhanced intensities of these high energy particles during SPEs increase the likelihood of particle impact to a susceptible site on the device. Total dose effects, or the increase in fluence experience by a spacecraft as the result of an SPE, can abbreviate spacecraft operational lifetimes by saturating design thresholds in short bursts of radiation.

By correlating a database of spacecraft anomalies with the daily and hourly space weather parameters, Iucci et al., (2005) found that these occurrences are associated with greater than 10 MeV solar energetic protons with intensities greater than 1000 particles $cm^{-2}s^{-1}sr^{-1}$ (pfu), while proton intensities less than 100 pfu have a negligible correlation to such events.

1.1.2 Threats posed by SEPs to biological systems

The potential effect of solar energetic particle events on astronauts in space is dependent on the energy threshold required for a particle to penetrate protective shielding and destroy tissue. This threshold is roughly at 20 – 40 MeV/nucleon (Posner, 2007). At this energy, protons and helium nuclei are the particle species most threatening sensitive organs in the human body because they have the greatest penetration length. Penetration length, the thickness of material an energetic particle can pass through, and is inversely proportional to ion mass. The onset of large intensities of ~30 MeV protons delivers large acute doses of ionizing radiation, which can cause acute radiation syndrome: vomiting, burns, and blindness (Townsend, 2005).

Passengers in airplanes traversing the Polar Regions can also be exposed to high doses of ionizing radiation from SPEs. As energetic charged particles enter the Earth's magnetic field, they are guided along field lines to the poles where they can enter the atmosphere. Aircraft do not have the same shielding as spacecraft designed for human flight, and changes in the Earth's magnetic field configuration due to disturbances in the interplanetary medium (geomagnetic

storms) can have a profound effects on SEP atmospheric radiation exposure (Mertens et al., 2010). Mitigation of this threat usually requires the diversion of flights to lower latitudes.

1.2 NOAA Space Radiation Storm Scale

In order to convey the correlation between space weather event intensity and probable impacts on systems in space, the NOAA-SWPC developed a space weather scale to classify severity of space weather events, analogous to the Richter scale for earthquakes (Poppe, 2000). This logarithmic scale, adapted in Table 1, give a rough idea of the affects on biological systems, satellite operations, and RF communications from greater than 10 MeV particle events. The final column in the table provides a sense for how common events of these magnitudes are over one solar cycle (~11 years).

Solar Radiation Storms				
Category		**Effect**	**Physical measure**	**Average Frequency**
Scale	**Descriptor**	**(Duration of event will influence severity of effects)**	**Intensity level of >= 10 MeV particles (ions)***	**number of days per cycle**
S5	**Extreme**	**Biological:** unavoidable high radiation hazard to astronauts on EVA (extra-vehicular activity); passengers and crew in high-flying aircraft at high latitudes may be exposed to radiation risk.*** **Satellite operations:** satellites may be rendered useless, memory impacts can cause loss of control, may cause serious noise in image data, star-trackers may be unable to locate sources; permanent damage to solar panels possible. **Other systems:** complete blackout of HF (high frequency) communications possible through the polar regions, and position errors make navigation operations extremely difficult.	10^5	Fewer than 1 per cycle
S 4	**Severe**	**Biological:** unavoidable radiation hazard to astronauts on EVA; passengers and crew in high-flying aircraft at high latitudes may be exposed to radiation risk.*** **Satellite operations:** may experience memory device problems and noise on imaging systems; star-tracker problems may cause orientation problems, and solar panel efficiency can be degraded. **Other systems:** blackout of HF radio communications through the polar regions and increased navigation errors over several days are likely.	10^4	3 per cycle
S 3	**Strong**	**Biological:** radiation hazard avoidance recommended for astronauts on EVA; passengers and crew in high-flying aircraft at high latitudes may be exposed to radiation risk.*** **Satellite operations:** single-event upsets, noise in imaging systems, and slight reduction of efficiency in solar panel are likely. **Other systems:** degraded HF radio propagation through the polar regions and navigation position errors likely.	10^3	10 per cycle
S 2	**Moderate**	**Biological:** passengers and crew in high-flying aircraft at high latitudes may be exposed to elevated radiation risk.*** **Satellite operations:** infrequent single-event upsets possible. **Other systems:** small effects on HF propagation through the polar regions and navigation at polar cap locations possibly affected.	10^2	25 per cycle
S 1	**Minor**	**Biological:** none. **Satellite operations:** none. **Other systems:** minor impacts on HF radio in the polar regions.	10^1	50 per cycle

Table 1.1 - NOAA classification scheme for SPEs (Poppe, 2000). Events are categorized based on maximum intensity level of >10 MeV ions.

2 Forecasting Basics

The onsets of hazardous solar particle events using *in situ* particle data are highly dependent on local plasma conditions between the Sun and 1AU, which govern particle propagation. Understanding these conditions and how they affect the observations of SEPs at Earth is crucial to the development of a forecasting algorithm.

Since the 1980's, the persistent paradigm for SEP characterization has divided SPEs into two categories, impulsive and gradual, distinguished initially by temporal extent, with impulsive events spanning hours and gradual events spanning days. Impulsive events tend to have abundance enhancements of high Z elements, enrichments of He^3/He^4, and extreme ionization states, characteristic of flare heated material. While these events are often effective accelerators of near-relativistic electrons, they are rarely accompanied by high energy (>10 MeV) protons. Gradual events tend to have compositions characteristic of coronal abundances, and exhibit a good correlation between peak particle intensity and associated coronal mass ejection (CME) speed [(Cane et al., 1986), (Reames, 2001)]. Compositional studies of impulsive and gradual events have blurred the distinction of this classification scheme, indicating that flare material maybe reaccelerated at CME shock-fronts (Cohen et al., 1999).

According to Cane et al. (1988) the time-intensity profile of gradual SEP events takes different forms depending on event strength, solar longitude of the source region, and energy of observation. The shape of the time-intensity profile of a solar particle event is largely determined by the longitude of the solar event relative to the observer and is affected by the presence and strength of an interplanetary shock. West limb events display peak particle intensities early in the event as particles stream away from the shock front. Central meridian events show similar

onsets, but may have a secondary peak days later when the shock arrives. East limb events are dominated by diffusive particle transport and consequently display a more gradual onset. The shock-fronts associated with East limb events are rarely observed at Earth. Figure 2.1 is a visual representation of event profile variability as a function of solar longitude, measured at 1AU.

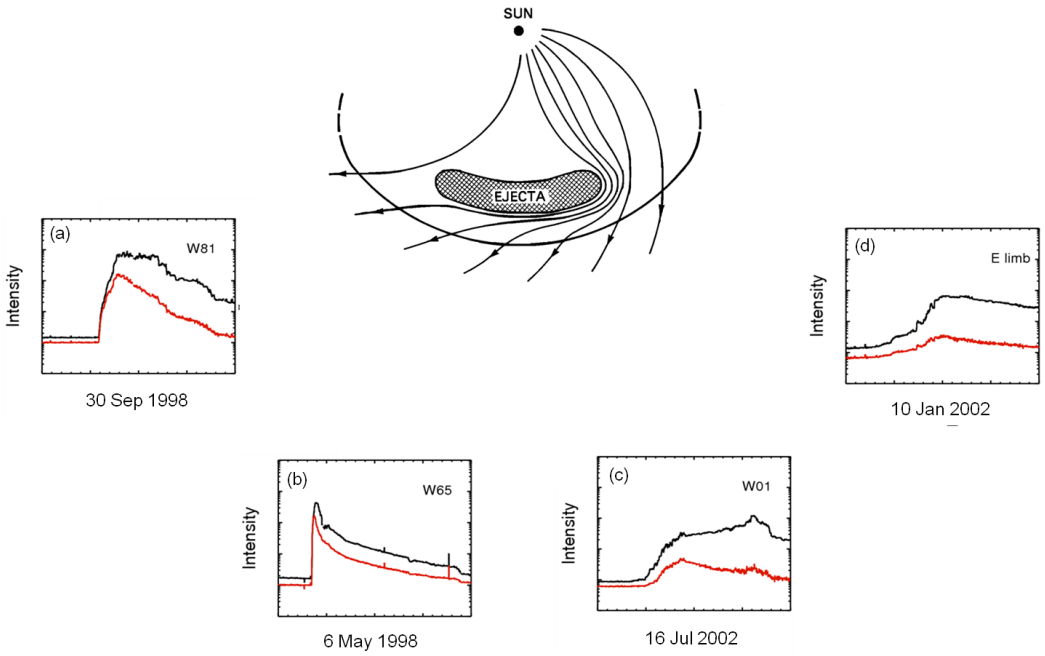

Fig 2.1 – Depiction of variability in the time-intensity profiles of >10 MeV (black) and >30 MeV (red) protons as measured by the Solar Isotope Spectrometer on ACE (see Section 3.2. for discussion of this instrument) as it depends on associated flare location, indicated in the upper right-hand corner of each profile. Figure adapted from Cane et al. (1988)

2.1 Solar Energetic Particle Propagation in the Inner Heliosphere

In order to explain the variability in the time-intensity profiles of proton events, we must understand the basics of particle propagation in the inner heliosphere. The solar wind, a constant stream of low energy particles off the solar corona, permeates interplanetary space. As the solar wind spreads out into the interplanetary medium, it carries with it the solar magnetic field. This field is said to be "frozen-in" to the expanding plasma and is drawn out past the planets while the

footprints of these field lines remain connected to the solar surface. The magnetic field carried out from the Sun by the solar wind into interplanetary space is known as the Interplanetary Magnetic Field (IMF). The radial outflow of the solar wind coupled with solar rotation twists these field lines into the canonical Parker spiral (Parker, 1965). At 1AU, this result is observed as a magnetic field that intersects Earth's orbit at a roughly 45° angle to the radial, as described by $\tan \emptyset_r = \frac{r\,\Omega_\odot}{V_{sw}}$, where $\emptyset_r$ is the magnetic field direction relative to the radial, $\Omega_\odot$ is the rotation rate of the sun (1 revolution per 27 days), r is the radial distance (1AU), and V_{sw} is the solar wind speed (typically around 400-500 km s^{-1}). Nominally, field lines which are well-connect to the Earth have their footprints at solar longitudes of approximately W60.

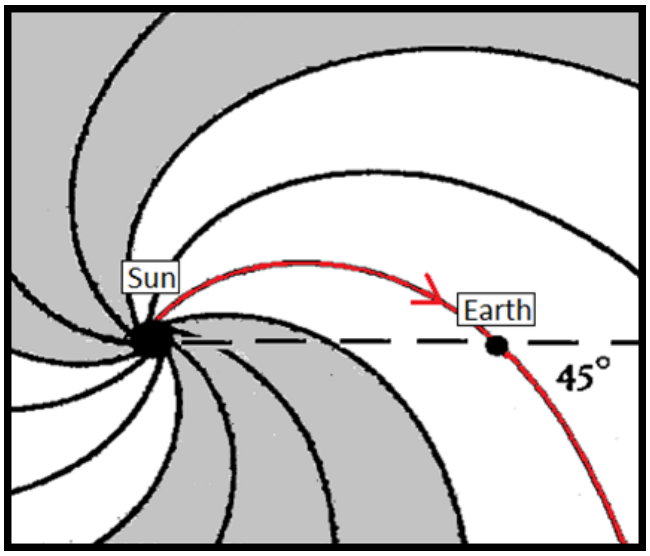

Fig 2.2 – Illustration of Parker spiral viewed in ecliptic plane. Solar field lines are carried out past the Earth and twisted into the form of an Archimedean spiral. The heliospheric current sheet warps, resulting in regions of opposite polarity, indicated in gray. "Well-connected" field line, which connects to approximate W60, is shown in red.

Magnetic reconnection, which converts magnetic potential energy into plasma kinetic energy, is believe to be an efficient mechanism for particle acceleration in both impulsive and gradual events. While the details of magnetic reconnection that underlie both flare and CME acceleration are still poorly understood, once energetic protons escape, under scatter-free conditions, they are guided by these spiral interplanetary field lines with gyroradii determined by particle mass and charge (*m/q*). Those particles injected onto field lines which are "well-

connected" to Earth, as shown in red in Figure 2.2, travel roughly 1.2 AU and result in a prompt onset, exemplified in Figure 2.1(b). Under ideal, scatter-free propagation conditions, the transit time along this path is determined by particle speed. A simple calculation reveals that it should take 10 MeV protons roughly 69 minutes to reach the Earth once they have been released from the Sun. Particle onset times at a given total energy measured at 1AU will therefore be species dependent.

Particles injected onto field lines which are "poorly connected" cannot take as direct of paths to reach the Earth. These particles must diffuse across field lines, resulting in a time intensity profile that exhibits a much more gradual onset, as in Figure 2.1(c,d). As noted by Reames et al. (1996), a slow rising event is not indicative of weak or inefficient shock acceleration, but of East limb events.

2.2 Previously developed Forecasting Models

There are currently a variety of operational methods in place to forecast solar particle events. These methods utilize *in situ* data (differential and integral particle intensities), remote data (radio emission, x-ray intensities), or a combination of the two. Prediction models that use flare signatures instead of *in situ* data have temporal forecasting advantages when diagnosis is made during the particle injection phase rather than after propagation to 1AU. However, using purely remote data has the disadvantage that it does not sample the dynamic state of the interplanetary medium. Forecasting schemes presented by Posner (2007) and Núñez (2007) utilize purely *in situ* data while those presented by Kahler et al. (2007), Balch (2008) and Laurenza et al. (2009) rely on a combination of *in situ* and remote data.

2.2.1 Purely *in situ* forecasting methods

In his study of 65 GOES 8 > 10 pfu Particle Events from 1996 to 2002, Posner (2007) demonstrates the possibility of forecasting the appearance and intensity of solar ion events by means of relativistic electrons, providing lead times of up to one hour. By considering the differential intensity of 0.3-1.2 MeV electrons and its rate of rise for each minute of data over this seven year period, he constructs a forecasting matrix used to predict proton intensity one hour later. This approach achieves high forecasting effectiveness for 30-50 MeV proton events with peak intensities greater than 30 pfu, successfully predicting 100% (4 out of 4) of events with 44% (4 out of 9) prediction probability when applied to data from 2003. Posner's demonstration of the feasibility of exploiting the shorter transit time of electrons relative to ions to predict proton onset was the impetus for this study. For our extension of Posner's prediction method to a lower energy regime using data from the Advanced Composition Explorer, see Appendix A.

UMASEP (Núñez, 2007) is a dual-model system, which distinguishes between event profiles resulting from magnetically well-connected and poorly-connected geometries. Núñez's "Well-Connected SEP Forecasting Model" estimates magnetic connectivity by correlating the time derivatives of differential 9-500 MeV proton intensity channels with the time derivative of soft x-ray intensity. An event prediction is triggered if magnetic connection is present and associated flare intensity is greater than 7×10^{-6} Wm^{-2} (C7 flare). The "Poorly-Connected SEP Forecasting Model", active when correlation between x-ray intensity and proton intensity time derivatives is low, relies on pattern recognition of time-intensity profiles of the low-intensity differential proton flux, trained on data from solar cycles 22 and 23. Nùñez's implementation of

a combination of complementary forecasting models to more specifically engineer prediction schemes to different event profiles has been adapted for this study.

2.2.2 Combination *in situ* and remote forecasting methods

For over three decades, the Proton Prediction System (PPS) and PROTONS endured as the principle SEP forecasting systems [(Kahler, Cliver, & Ling, 2007), (Balch, 2008)]. The PPS assumes flare acceleration as the generator for SEPs, using peak flare intensity, flare location, and time integrated x-ray and radio intensity to estimate proton intensity. Used as a decision aid by human forecasters at NOAA/SWPC, PROTONS also assumes flare acceleration, but includes the potential for shock acceleration by monitoring the occurrence of type II and type IV radio emissions, indicating the presence of a CME shock propagating through the solar corona.

Laurenza et al. (2009) look for evidence of particle acceleration and escape based on flare longitude, time-integrated soft x-ray intensity, and time-integrated type III radio emission, issuing warnings after the observation of an associated M2 or greater flare. It should be noted that those prediction schemes which rely on soft x-ray data are fundamentally limited because of their basis on the proxy association between SPEs and flares. Only Posner bases his method solely on particle data, rather than relying on proxies. Another key shortcoming of these prediction schemes (other than PROTONS) is that in estimating peak proton intensity during an SEP, the potential for shock enhancements to proton intensity is omitted, a feature which, if present, is potentially the most hazardous component of an SPE.

This study presents the development of a forecasting scheme that, like Posner's, relies only on *in situ* particle evidence, and, like Nùñez's, attacks the prediction of well-connected and poorly-connected events by complementary methods.

3 Instrumentation

This study focuses on the use of purely real-time *in situ* observation as the basis for forecasting the onsets of solar particle events. All of our data were taken from ACE, the Advanced Composition Explorer, a solar observing spacecraft, which houses an array of scientific instruments designed to take *in situ* energetic particle measurements and monitor the state of the interplanetary medium through solar wind and magnetic field characterization. This satellite resides in a Halo orbit about L1, the Sun-Earth libration point, about 1.5 million km sunward of Earth (Stone, Frandsen, et al., 1998). This location, unblocked by the Earth or its magnetic field, is ideal for making observations of the Sun, and its position inside of 1AU allows it to encounter events before they reach the Earth. ACE is spin stabilized, completing one rotation about every 12 seconds, with is spin axis approximately oriented in the sunward direction. The ACE satellite provides raw space weather data to NOAA's Real-Time Solar-Wind (RTSW) system within 5 minutes of measurement at the spacecraft (Zwickl, 1998). The immediate availability of this data makes it ideal for the purpose of monitoring interplanetary space weather.

Accurate determination of the relative arrival times of different particle species is crucial to this study. Therefore, it made sense to use data taken from instruments on the same spacecraft. Electron and proton intensity were provided by EPAM and SIS, respectively, while MAG and SWEPAM provide contextual data regarding the condition of the interplanetary medium.

3.1 Solar Isotope Spectrometer (SIS)

The Solar Isotope Spectrometer (SIS) is designed to measure energetic nuclei from Z = 1 (H) to Z = 30 (Zn) in order to characterize isotopic composition of solar energetic particles (Stone, Cohen, et al., 1998). This large area, solid state spectrometer has a 95° field of view and geometrical factor of 38.4 cm^2 sr. Using the deposited energy and residual energy (dE/dx - E technique discussed in Appendix C), along with particle trajectory, provided by an on-board hodoscope, SIS provides mass resolution of 0.25 amu or better. Because this instrument was designed to be discerning of heavy nuclei, the integral intensity of high energy protons is a secondary data product and available as "Browse Data" from the ACE Science Center: <http://www.srl.caltech.edu/ACE/ASC/ browse/view_ browse_data.html>.

This data product, which conveniently align well with the hazard levels discussed in Section 1 for electronic and biological systems in space. It should be noted that during times of high intensities of low energy protons, SIS preferentially selects Z > 10 events for analysis and may not accurately transmit the proton intensities of interest to this study. Furthermore, during quiet time, SIS proton intensities are contaminated by particles entering from the sides of the detector, resulting in high background intensity. See Appendix B for more details regarding how these ACE-SIS proton intensity inaccuracies affects our analysis.

3.2 Electron, Proton, and Alpha Monitor (EPAM)

The Electron, Proton, and Alpha Monitor (EPAM), a flight spare of the Ulysses Hi-SCALE instrument, is designed to characterize the transient behavior of electrons (40 - 350 keV) and protons (0.046 - 4.8 MeV) associated with solar flares and coronal mass ejections (Gold et al., 1998). Its five telescopes provide coverage of almost the entire unit sphere over a rotational

period. For this study, we used the Low Energy Foil Spectrometer (LEFS60), a sub-telescope pointed 60° from the spacecraft spin axis with a cone angle of 53° and geometry factor of 0.397 cm^2 sr. LEFS is designed to capture electrons greater than 45 keV by blocking out ions less than 350 keV with an aluminized Parylene foil. A totally depleted, solid-state silicon detector measures the deposited energy of incident to bin the particles into four energy channels. Because the LEFS electron energy channels may be contaminated by ions which penetrate the foil, we have compared the electron intensities measured in LEFS60 to the deflected electrons channel from EPAM/LEMS30. A discussion of this investigation can be found in Appendix D.

Energy Channel	Passband (MeV)	Species
E1'	0.045-0.062	electrons
E2'	0.062-0.103	electrons
E3'	0.103-0.175	electrons
E4'	0.175-0.312	electrons
FP5'	0.546-0.761	ions
FP6'	0.761-1.22	ions
FP7'	1.22-4.97	ions

Table 3.1 – Energy channels and passbands for the LEFS60 telescope on ACE/EPAM

For this study, we used electron count rates from channels E4' and E3'. The data from the EPAM instrument is available at: <http://data.ftecs.com/VHO/VEPO/ace_epam/rates/>. Using count rates at a 12-second cadence we calculated the one-minute differential intensities (particles $cm^{-2}s^{-1}sr^{-1}MeV^{-1}$) that were used for this study. For more information regarding EPAM, including anti-coincidence logic, calibration, and in-flight instrument performance see Gold et al. (1998).

3.3 Magnetic Field Data

The Magnetic Fields Experiment (MAG) provides time-varying measurements of the local interplanetary magnetic field (IMF) using two boom-mounted fluxgate sensors on opposite

solar panels (along the +/- Y axis of the spacecraft) (Smith et al., 1998). This data is un-spun and rotated into useful coordinate systems, and released as a "Level 2" verified data product on the ACE Science Center: <http://www.srl.caltech.edu /ACE/ASC/level2/index.html>. We have used the 64-second cadence magnetic field data in heliocentric (RTN) coordinates throughout this study.

To augment our study of this magnetic field data, we use the "Near-Earth Interplanetary Coronal Mass Ejections in 1996-2007" produced as a "Level 3" data by Richardson and Cane. In particular we note the passage of shocks, Interplanetary Coronal Mass Ejections (ICMEs), and Magnetic Clouds (MCs), to provide context for particle acceleration. These lists can be found at: <http://www-ssg.sr.unh.edu/mag/ace/ACElists /obs_list.html>.

3.4 Solar Wind Data

In addition to particle abundances, ACE tracks real-time *in situ* solar wind parameters to include: solar wind speed, temperature, and proton density, provided by the Solar Wind Electron Proton Alpha Monitor (SWEPAM) (McComas et al., 1998). These parameters, which characterize local plasma conditions, can give us an idea of when the interplanetary medium as been disturbed by solar activity and indicate the passage of shocks. However, we find that when considered with EPAM and SIS data, there is not a direct connection between instantaneous solar wind conditions and later SEP onset. A discussion of this analysis is given in Appendix E.

4 Overview of > 10 MeV Proton Events

The time-intensity profiles of SPEs are highly variable, making it difficult to describe a characteristic form. There are, however, key parameters which can be used to characterize event profiles. This section presents an overview of relevant greater than 10 MeV proton event characteristics and discusses their distribution within the event population.

4.1 Event Selection

The National Weather Service Space Weather Prediction Center (SWPC) maintains a list of Solar Energetic Proton Events affecting the Earth Environment (http://www.swpc.noaa.gov/ftpdir/indices/SPE.txt) as observed by the GOES spacecraft. According to this list, an event is defined as any instance where the integral 5-minute averaged intensity of greater than 10 MeV protons exceeds 10 pfu (1 pfu = 1 particle $cm^{-2}s^{-1}sr^{-1}$). Because GOES spacecraft reside in geosynchronous orbit about the Earth, while the ACE spacecraft orbits 1.5 million km sunwards of Earth, we expect the measured > 10 MeV proton intensity to differ between these two, but be consistent within an order of magnitude. See Appendix B for an explanation of order of magnitude inconsistencies between these two satellites.

Using ACE-SIS > 10 MeV integral proton intensity, we constructed our own event list, setting a threshold of 30 pfu for event selection. We consider any solar particle event in which the >10 MeV proton intensity exceeds 30 pfu for at least 15 minutes to be a "critical event". This threshold was chosen based on the Solar Radiation Storm hazardous intensity levels discussed in Section 1.2 which indicate negligible affects to biological systems and satellite operations for >10 MeV ion intensities $>10^2$. Because the distribution of these events as a function of intensity behaves as a power law, ignoring events below 30 pfu significantly reduces the number of events

we must examine, focusing our investigation on only the most hazardous events. The time period of interest covers events from 1998 – 2006.

Table 4.1 is a complete list of the "Critical Events" considered meaningful to this study. An event is delineated as at least 3 consecutive data points (15 minutes) of proton intensity greater than 30 pfu. The end of the event is defined once the proton intensity drops below 30 pfu. This classification forces events with time-intensity profiles that exhibit multiple onset phases without the integral intensity falling below 30 pfu to be grouped into one event. Further work would be needed if attempting to resolve multiple injections within a single event.

ACE "CRITICAL EVENTS"

Event #	Year	DOY	Proton Start Date	Proton Onset Time	Max Proton Intensity (pfu) (ACE/SIS)	Max Proton Intensity (pfu) (GOES)	Proton Onset Duration (min)	Associated Active Region Long.
1	1998	110	20-Apr	11:04	1318*	1700	225	W90
2	1998	122	2-May	13:53	160	150	20	W15
3	1998	126	6-May	8:22	436	210	5	W65
4	1998	236	24-Aug	22:37	167*	670	75	E07
5	1998	273	30-Sep	14:08	882	1200	90	W81
6	1998	318	14-Nov	6:26	218*	310	30	W90
7	1999	152	2-Jun	20:05	35	48	710	-
8	1999	155	4-Jun	8:12	51	64	85	W69
9	2000	49	18-Feb	21:42	46	13	70	E07
10	2000	95	4-Apr	16:56	56	55	630	W66
11	2000	158	6-Jun	21:33	65	84	1595	E18
12	2000	162	10-Jun	17:21	134	46	20	W38
13	2000	196	14-Jul	10:36	4382*	24000	10	W07
14	2000	256	12-Sep	13:38	208	320	260	W09
15	2000	313	8-Nov	23:16	4796**	14800	25	W75
16	2000	329	24-Nov	5:43	646	940	655	W05
17	2001	28	28-Jan	17:03	51	49	465	W59
18	2001	92	2-Apr	22:32	1022	1110	55	W82
19	2001	99	9-Apr	16:02	229	355	1130	W09
20	2001	105	15-Apr	14:00	1813	951	15	W85
21	2001	108	18-Apr	2:47	385	321	30	W limb
22	2001	228	16-Aug	0:31	536	493	35	back
23	2001	267	24-Sep	11:41	3705**	12900	95	E23

24	2001	274	1-Oct	12:57	1493	2360	20	W91
25	2001	308	4-Nov	16:42	4745**	31700	25	W18
26	2001	326	22-Nov	21:02	3652**	18900	165	W34
27	2001	360	26-Dec	5:41	1218	779	20	W54
28	2001	363	29-Dec	1:56	47	76	310	E90
29	2001	364	30-Dec	12:20	71	108	800	-
30	2002	10	10-Jan	11:12	67	91	590	E limb
31	2002	75	19-Mar	1:07	37	53	4500	-
32	2002	111	21-Apr	1:37	2093	2520	15	W84
33	2002	142	22-May	6:06	1150	820	970	W56
34	2002	188	7-Jul	12:32	30	22	410	W limb
35	2002	197	16-Jul	11:57	121	234	520	W01
36	2002	234	22-Aug	2:32	32	36	120	W62
37	2002	236	24-Aug	1:27	314	317	20	W90
38	2002	249	6-Sep	3:12	208	208	2115	E28
39	2002	313	9-Nov	15:02	428	404	340	W29
40	2003	148	28-May	2:41	80	121	2030	W17
41	2003	299	26-Oct	17:51	417	466	35	W38
42	2003	301	28-Oct	11:31	5820**	29500	40	E08
43	2003	306	2-Nov	17:42	1863	1570	5	-
44	2003	308	5-Nov	22:02	251	353	30	W83
45	2003	336	2-Dec	13:03	115	86	160	W limb
46	2004	102	11-Apr	5:12	33	35	495	W47
47	2004	207	25-Jul	16:17	1296	2086	160	W33
48	2004	257	13-Sep	10:17	277	273	615	E42
49	2004	263	19-Sep	17:37	76	57	140	W58
50	2004	306	1-Nov	6:07	129	63	20	backside
51	2004	312	7-Nov	10:06	472	495	550	W17
52	2005	15	15-Jan	6:57	3256	5040	1130	W05
53	2005	133	13-May	18:26	2251	3140	670	E11
54	2005	167	16-Jun	20:32	89	44	85	W87
55	2005	194	13-Jul	15:32	145	134	1380	W80
56	2005	206	27-Jul	17:21	56	41	3335	W90
57	2005	234	22-Aug	2:17	395	330	1080	W60
58	2005	250	11-Sep	19:41	1513	1880	370	E89
59	2006	339	5-Dec	13:47	2040	1980	1775	E79
60	2006	347	13-Dec	2:52	1453	698	10	W23
61	2006	348	14-Dec	22:47	70	-	5	-

*ACE-SIS proton data incomplete (missing) during event
** ACE-SIS <10 MeV proton intensity "saturated". See Appendix B for discussion.

Table 4.1 – Selected >10 MeV proton events from 1998 – 2008 based on SIS integral proton intensity measurements. GOES maximum integral proton intensity and associated active region were established using the list of GOES proton events at http://www.swpc.noaa.gov/ftpdir/indices/SPE.txt. Those events with proton onset duration times indicated in red are immediate events, as defined in Section 4.3

4.2 Key Parameters of >10 MeV Proton Events

(1) Event Onset Times

Proton onset times were established individually by selecting the first minute of observable increase above background for each particle species. 54 out of 61 events have well-resolved onset times, un-obscured by previous intensity enhancements, and abrupt enough to be definitively observed.

(2) Event Strength

Event strength indicates the threat level associated with a given event. The strength of a proton event can be characterized in two ways: (1) maximum >10 MeV proton intensity and (2) total event fluence. The benefit of using maximum intensity to define event strength is its simplicity; however, this approach merely samples minute in time of an event which may stretch over days. On the other hand, total fluence, the time-integral of proton intensity over the entirety of the event, is a more difficult metric to work with because it forces us to precisely define event start/stop times, which may not always be clear when multiple event occur in a short span of time. These two parameters pertain to different space weather concerns. Peak intensity is more descriptive when considering the single event effects energetic ions on spacecraft, while total fluence is the parameter of concern when discussing radiation dosing to humans in space. For this study we will use maximum integral proton intensity as a metric of event strength. Figure 4.1 shows the distribution of event strength for the 61 critical events listed in Table 4.1 as observed by both ACE-SIS and GOES.

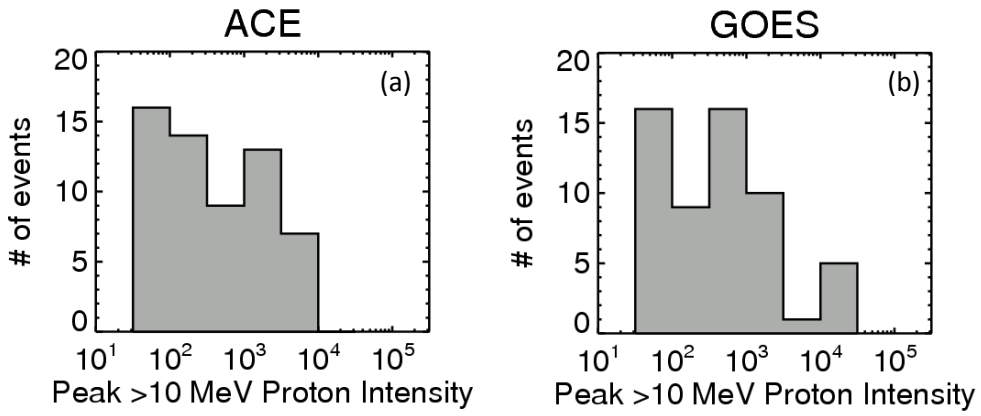

Fig 4.1 - (a) Histogram of event intensity as observed by ACE (b) Histogram of event intensity observed by GOES for the same events. The discrepancy (lack of ACE proton event greater than 10^4) is explained in Appendix B.

When looking at the time-intensity profile for a particularly well-connected event, to first order, we expect a rapid onset followed by a slow, exponential decay. This would indicate that the maximum event intensity would occur at the end of the onset phase. However, in many cases, these particles are associated with coronal mass ejections (CMEs), magnetic structures which propagate into the slower solar wind, potentially giving rise to shock fronts which take several days to reach 1AU. Particle populations trapped near a shock front by self-generated Alfvén waves, known as energetic storm particles (ESPs) may result in a spike in intensity greater than the initial onset intensity (Cohen, 2006). Figure 4.2 gives examples of both shock-related and non-shock-related maxima as observed by ACE-SIS.

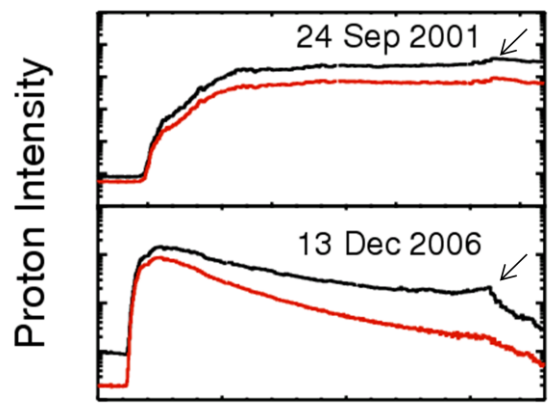

Fig 4.2 – (Top Plot) The event on 24 Sep 2001 is an example of a shock associated maximum, which occurs a day and a half after the initial onset, accompanying the passage of a shock. (Bottom Plot) The event on 13 Dec 2006 is an example of a shock accelerated enhancement which does not exceed the initial maximum attained at event onset. In both, >10 MeV protons are plotted in black, while >30 MeV protons are plotted in red.

When discussing the maximum integral intensity of an event, we will specify whether the maximum occurs at the event onset or if it is shock associated. We find that 14 out of 60 events have shock associated maximum proton intensities. Of these 14 events, only 7 exhibit prompt onset, followed by a decay phase and shock arrival days later. This lack of enhancement in high energy (>10 and >30 MeV) protons accompanying the interplanetary shock is to be expected as higher energies escape before the shock reaches 1AU (Li, Zank, & Rice, 2005). The other half of these events have extended onsets, which peak at the passage of the shock, indicating poor magnetic connection, likely originating near central meridian. We expect no shock-related particle enhancement from East limb events, because for this geometry, shocks are not seen at Earth.

(3) Event Onset Duration

We define event onset duration as the amount of time it takes for the proton intensity to reach 30 pfu once it begins to increase above the background intensity (nominally about 1 pfu). Figure 4.3 depicts the distribution of proton onset times for >10 MeV events. Although onset duration itself does not affect the type of threat associated with an event, it is an important parameter for assessing the amount of response time available for a given event. The shorter the event onset duration, the less time decision makers have to act on an event, making it more operationally imperative that these events be predicted ahead of time. We identify events with onset durations less than two hours as "immediate events". There are 28 immediate events in solar cycle 23.

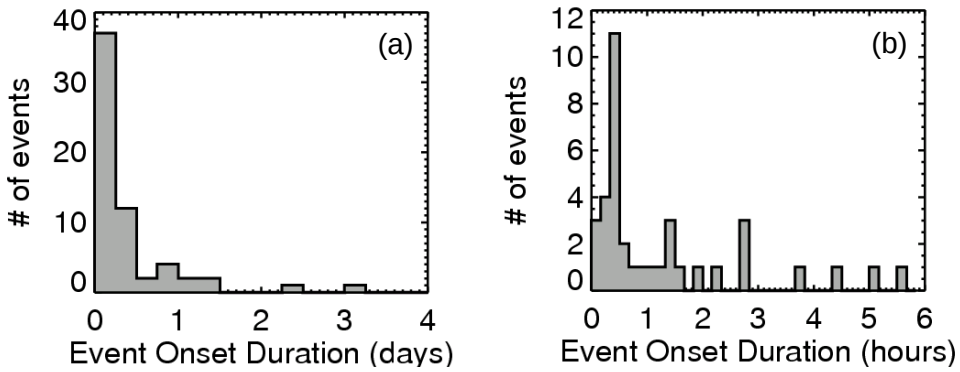

Fig 4.3 - (a) Histogram of event rise time, determined by the amount of time required for >10 MeV proton intensity to rise from background to >30 pfu, for the 61 events listed in Table 4.1. (b) Histogram of the 37 event with the most rapid proton onset. 28 events have onset durations less than 2 hours, defining them as immediate events.

(4) Magnetic Connection

Magnetic connection, as discussed in Section 2.1, has a significant impact on the time intensity profiles observed by ACE. While there are many factors affecting connectivity, including turbulence in the interplanetary plasma resulting from the passage of shock front and regions of high speed solar wind, we can use the associated flare location of a particle event as nominal metric for magnetic connection. We have approximate flare locations for most of those events registered by GOES as having a >10 MeV proton intensity greater than 30 pfu, provided on the Solar Energetic Proton Events List. Figure 4.4 depicts the correlation between solar longitude of flare location and maximum >10 MeV intensity received at GOES. One obvious feature of this figure is simply that particle events originating in the western hemisphere are more commonly observed at ACE than events originating in the eastern hemisphere. However, for this set of critical events which we have selected, solar longitude, in itself, does not seem to be a good indicator of maximum event intensity.

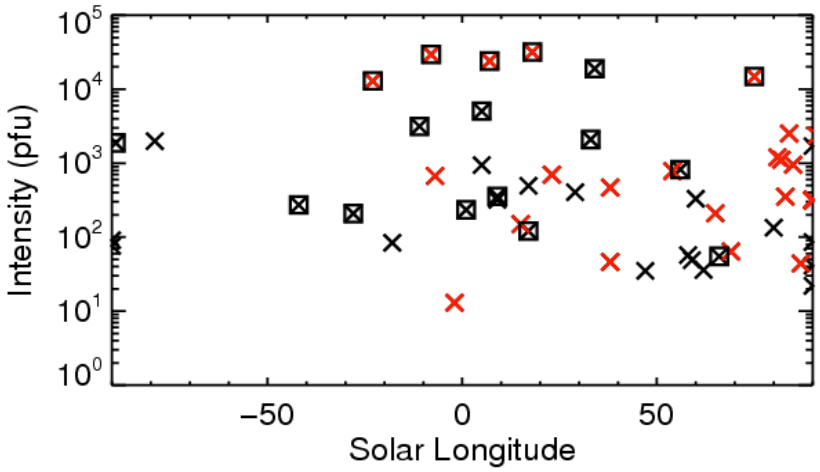

Fig 4.4 – Correlation between solar longitude of the event associated flare location and peak >10 MeV proton intensity measured by GOES. All 61 critical events are plots with x's. Those critical events with rise times less than 2 hours are indicated in read. Events over-laid with boxes have shock associated peak proton intensities. Most of these fast-rising events originate in the Western hemisphere of the Sun.

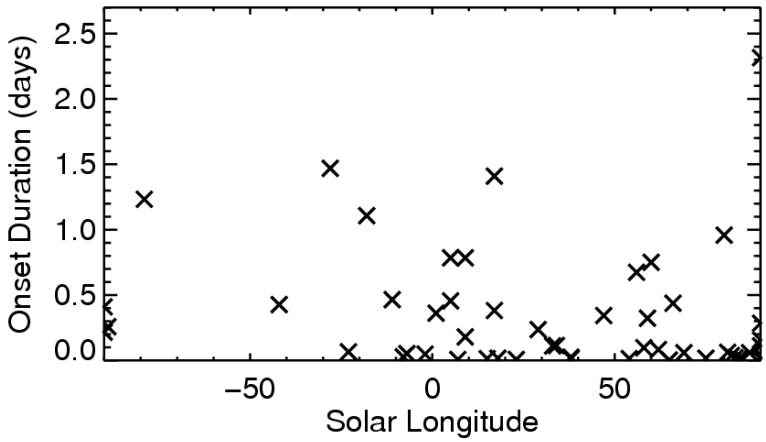

Fig 4.5 – Correlation between solar longitude of the event associated flare location and event onset duration. We notice a concentration of events of short onset duration between E10 and W90. However, across these solar longitudes, longer onset durations are observed as well.

4.3 Event Classification

Based on these three parameters (event intensity, onset duration, magnetic connectivity), we can classify events into three categories. This categorization scheme allows us to highlight

different time-intensity event profiles which we would like to design our prediction scheme to recognize.

1. Well-connected, fast-rising – Prompt, scatter-free onset of particles at 1 AU, followed by gradual decay, on the order of days. Proton onset times are less than 2 hours, classifying them as immediate events. As these events are usually magnetically well-connected, particle intensity is maximal for a given event strength and proton onset is unobscured. These events tend to have greater peak particle intensities. There are 23 events that exhibit this profile.
2. Poorly connected, slowly rising – Dispersive onset of particles at 1 AU. Event strength is observed from a less than maximal location. Particle intensity onsets on the order of hours and decays on the order of days. For some events, particle intensity increases gradually until the passage of a shock, and then decays. These events tend to have lower peak particle intensities. There are 31 events that exhibit this profile.
3. Follow-on events – Proton events which onset before the previous event has decayed to background levels. These complex events have various time intensity profiles, but share the common feature of an obscured event onset. A subset of these events may be immediate events; however, because these follow-on events often have complicated time-intensity profiles, we choose not to divide this group any farther. There are 7 events that have obscured proton onsets.

As event onset duration and magnetic connectivity are continuous parameters, this classification scheme is obviously over-simplified. The dividing line of a 2 hour onset time we have chosen for critical forecasting is an organizational tool, which allows us to categorize otherwise complicated profiles.

5 Electron Signatures in >10 MeV Proton Events

As discussed by van Hollebeke et al. (1975), energetic electrons are the first *in situ* evidence for the onset of a solar particle event, based on their velocity advantage during scatter-free propagation (discussed in Section 2.1). These particles carry with them critical information about the subsequent proton onset. In this section, we investigate the characteristics of the near-relativistic (NR) electrons that accompany >10 MeV proton events. The three electron properties we are interested in are: (1) electron intensity (2) electron rise parameter and (3) electron spectral ratio, described below.

5.1 Electron Event Intensity

Electron event intensity is defined as the maximum differential intensity reached in the highest energy channel (E4': 175 – 312 keV) of ACE-EPAM. There is a correlation between the maximum electron and proton intensities recorded in an event (Figure 5.1). It is important to note that these intensities may have occurred in different phases of the event and, therefore, may not have a direct physical relationship to one another. Haggerty & Roelof (2009) find a more unequivocal correlation between maximum electron and proton intensities by limiting their event selection to include only "beam-like" near-relativistic electron events and ignoring shock associated particle enhancements.

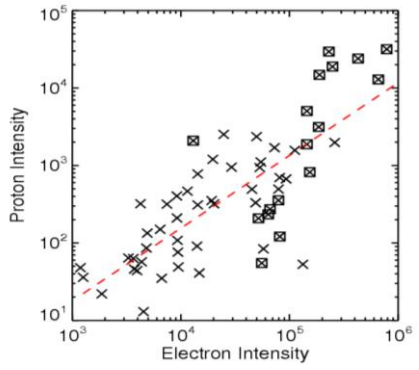

Fig 5.1 - Correlation between the maximum differential electron intensity and maximum integral proton intensity achieved for each event listed in Table 4.1. Below a maximum electron intensity of 2×10^5 particles $cm^{-2}s^{-1}sr^{-1}MeV^{-1}$, for a given electron intensity, proton intensity varies over several orders of magnitude. Note that all proton events identified in Section 4.1 are accompanied by a maximum electron intensity of at least 1×10^3 particles $cm^{-2}s^{-1}sr^{-1}MeV^{-1}$. Red trend-line indicates best fit linear correlation between electron and proton intensity in log-space.

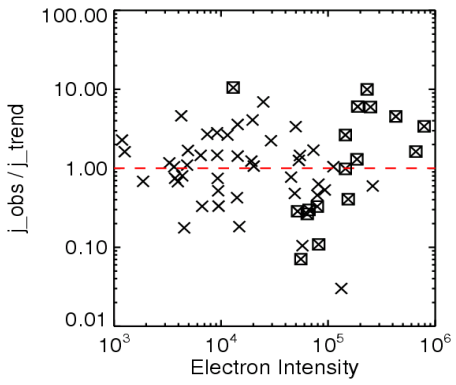

Fig 5.2 – Using the trend-line shown in Figure 5.2, we can determine a predicted proton intensity for a given electron intensity (j_trend). Comparing the observed proton intensity for each event to the predicted proton intensity (j_obs/j_trend), indicates the variation in proton intensity as a function of electron intensity. There may be orders of magnitude difference for a given electron intensity.

5.2 Electron Rise Parameter

In order to assist in the automatic identification of the onset of NR electrons, we define the electron rise parameter (Posner, 2007), which is effectively the inverse logarithmic rise time of the differential electron intensity, as specified by Equation 5.1.

$$\Phi_e = \frac{\mathrm{d}}{\mathrm{dt}}\left[\frac{\log_{10}(I_e(t=t_2))}{\log_{10}(I_e(t=t_1))}\right] \propto \frac{1}{\tau} \tag{5.1}$$

Using linear regression applied to the electron time intensity profile, we can define Φ_e for each minute of data by using that minute as the last minute in the fit (t_2) and including all of the data back to some time (t_1) in the fit. For this study we chose to use a "sliding" rise parameter to more accurately characterize the electron onset. This "sliding" rise parameter is calculated by allowing the fit to vary in length over a 10 minute window, from 4 to 13 minutes back in time. In all cases, the minute of interest is kept as the final data point in the fit. Out of these 10 fits, we choose the *largest* slope determined over this window and assign that slope as the rise parameter for that minute. Figure 5.2 shows a few examples of how this sliding rise parameter appears for a variety of electron time-intensity profiles.

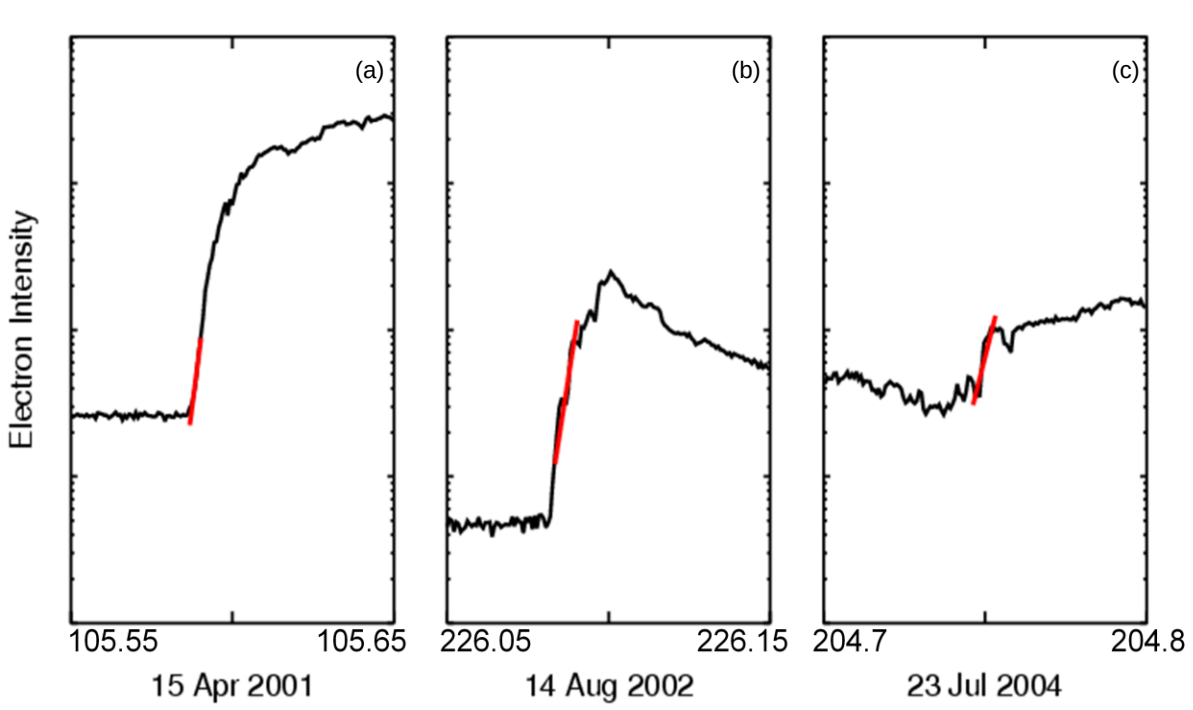

Fig 5.2 - (a) Classic (well-connected) onset: exponential rise of NR electrons followed by a gradual decay, on the order of days. (b) Spiked onset: sharp rise followed by steep decay, on the order of hours. Electrons with this time-intensity signature are usually not accompanied by large proton intensities (c) Jump in electron intensity produced by the passage of an interplanetary magnetic structure. Electron Intensity in units of particles $cm^{-2}s^{-1}sr^{-1}MeV^{-1}$. Each onset is plotted over a 4 hour period.

We note that, remarkably, for most magnetically well-connected events, the early phase of event onset is approximately linear such that $\tau = \tau_0 \exp(\alpha t)$, while the early phase of poorly connected events is more sporadic. Steep electron rise parameters can be achieved other times than the onset phase of an event. The particle population can fluctuate immediately as the spacecraft transits into distinct flux tubes, resulting in a discontinuity in electron intensity and a steep rise parameter, as shown in panel (c) of Figure 5.2. Steep rise parameters in this case are not associated with event onset but with the transition of the spacecraft into a new flux tube. Often, there is a simultaneous discontinuity in the strength of the interplanetary magnetic field. A successful prediction scheme must select against this type of feature.

5.2.1 Correlation between Electron Rise Parameter and Event Onset Duration

Both the electron rise parameter and the event onset duration provide information regarding the rate of onset of their particular species. While the proton onset duration is a single characteristic time for each event, the electron rise parameter is a continuously defined quantity. Both proton onset duration and electron rise parameter are, to some extent, a measure of the magnetic connectivity of an event. Therefore, we expect a correlation between these two parameters for a given event (Figure 5.3).

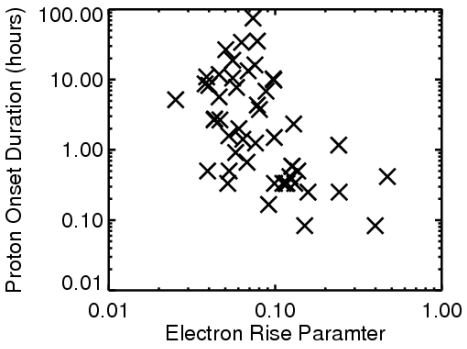

Fig 5.3 – Comparison of maximum electron rise parameter measured during the onset of the event to event onset duration for the 61 events listed in Table 4.1. Correlation between these two parameters is indicative the fact that electrons and protons share basically the same magnetic connection for a given event.

5.2.2 Correlation between Electron Rise Parameter and Event Strength

Figure 5.4 compares the maximum electron rise parameter achieved during the event onset to the proton event intensity. For those events with a maximum electron rise parameter below 0.2 $\frac{d \log(j)}{dt}$, peak proton intensities vary over four orders of magnitude. There appears to be little correlation between maximum electron rise parameter achieved during event onset and peak proton intensity.

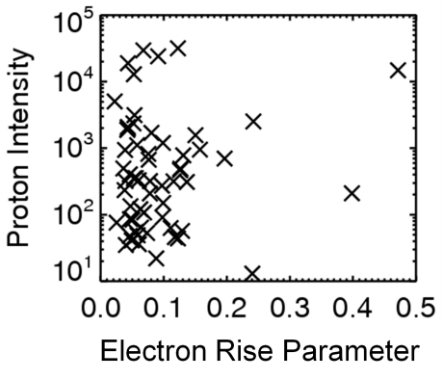

Fig 5.4 - Comparison of maximum >10MeV proton flux achieved during entire duration of event against maximum electron sliding rise parameter achieved during event onset for the 61 events listed in Table 4.1.

5.3 Electron Spectral Ratio

In order to provide a rough characterization of the spectrum of incident electrons, we define the electron spectral ratio: the ratio of the differential intensity in the second highest energy channel (E3': 103-175 keV) to that in the highest energy channel (E4': 175-312 keV) as given as $S = \frac{\Phi_{E3'}}{\Phi_{E4'}}$.

By defining this quantity for every minute of data, we can observe how the spectrum evolves with time as an event onsets and decays away. If this ratio increases with time, the spectrum of that event is softening (including relatively more low energy particles). If this ratio decreases with time, the spectrum is hardening (including relatively more high energy particles). The spectrum seen over the duration of a single event may be a good indicator of the injection location or mechanism of acceleration that generated these electrons (Haggerty & Roelof, 2009). However, we are interested in the instantaneous relationship between these two energy channels, rather than the accumulated spectrum. Because we are dealing with realtime data, the accumulated spectrum is not a parameter that is accessible to us at event onset.

5.3.1 Velocity Dispersion – Spectral Signature

In an event that exhibits scatter-free propagation of the earliest arriving particles, we should observe a velocity dispersion. The highest energy electrons (those traveling the fastest) should arrive first, followed by an increasing number of lower energy particles. Therefore, at the very beginning of a scatter-free event we expect a very hard spectral ratio followed by an immediate softening of this ratio. However, as particle counts are low at the very beginning of an event onset, the spectral ratio is an ill-defined measure. We observed this behavior clearly in 9 out of 61 events.

5.3.2 Spectral Signature of "Follow-On" Events

The main goal of exploring the behavior of this ratio over the course of an event is the identification "follow-on" events, those events which onset before the previous event has decayed to a background level. We observe 7 of these events during solar cycle 23. As the electron onset of these events is obscured, other means are necessary for identifying the arrival of another particle population. We believe that the time profile of the spectral signature satisfies this need. Figure 5.4 is an example of a follow-on event observed on 18 Apr 2001. These follow-on events are of particular interest because they propagate into a perturbed interplanetary medium, resulting in a modified event profile. Gopalswamy et al. (2004) note that, in their study of coronal mass ejections from solar cycle 23, higher SEP intensities result when a CME is preceded by another wide CME from the same source region.

We observe that in over half (35/61) of the solar proton events listed in table 4.1, there is a characteristic time profile for the electron spectral ratio (Figure 5.4). Following event onset, this parameter softens to a ratio of approximately 4.0, regardless of whether a distinct electron

velocity dispersion is observed in the early minutes of particle arrival. Then, as electron intensity decays, this ration hardens below 2.0, indicating that lower energy electrons decay more quickly than higher energy electrons. Therefore, we associate spectral ratios above 2.0 with the onset phase of an event, and spectral ratios below 2.0 with the decay phase of the event.

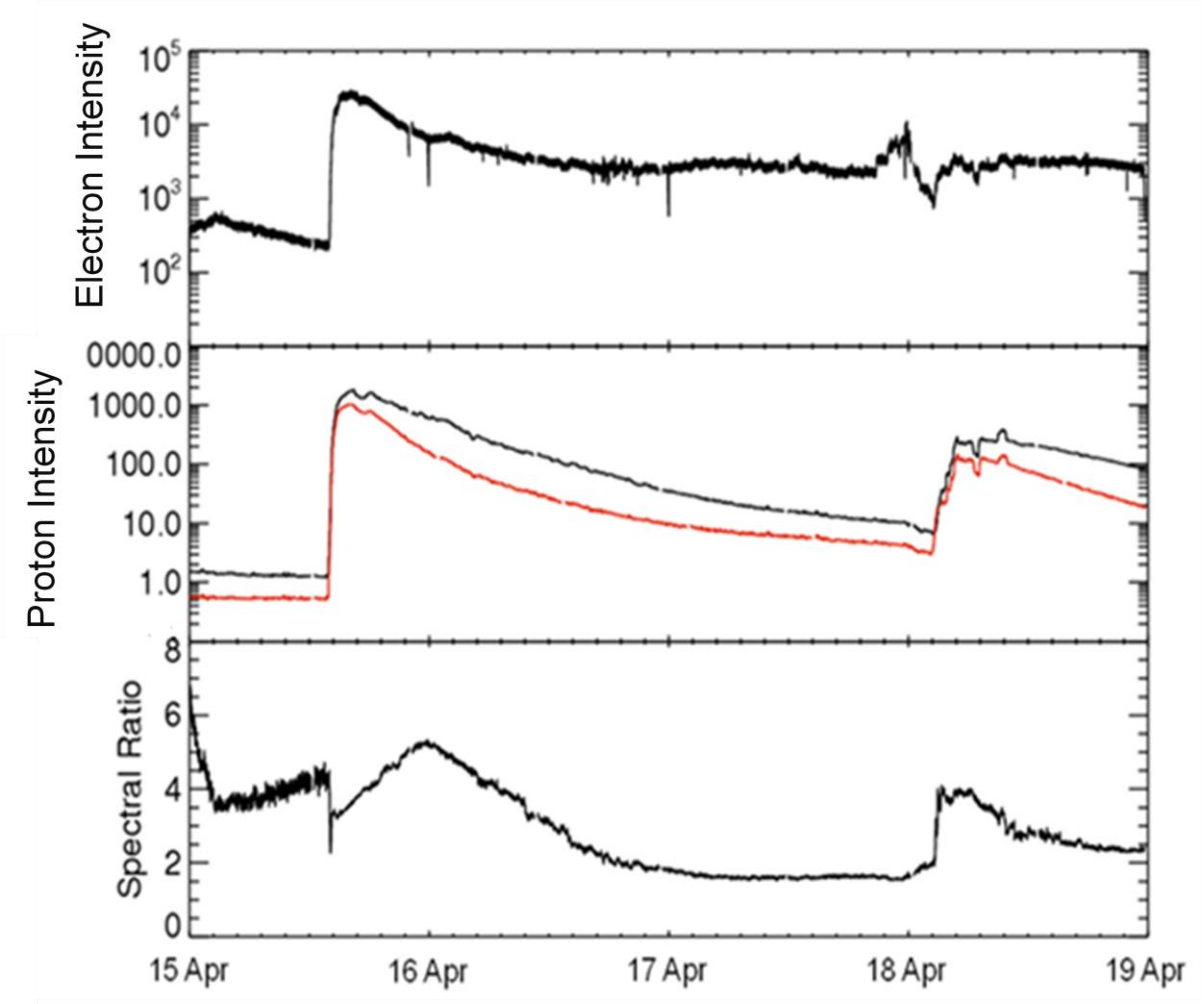

Fig 5.4 - Example "Follow-on" event (Events #20 and #21 from Table 4.1). Initial proton event onset on 15 Apr 2001 (DOY=105). By 18 Apr 2001 (DOY=108), proton intensity has decayed close to background levels while electron intensity remains elevated at 10^3 particles $s^{-1}cm^{-2}sr^{-1}MeV^{-1}$. The abrupt change in the spectral ratio observed at 02:35 on 18 April may indicate the arrival of a new particle population, more clearly than the differential electron from channel E4' alone.

6 The Algorithm

As discussed in Section 2.1, the time-intensity profiles of SEP proton events as observed by ACE are highly dependent on spacecraft location and magnetic connection. In Section 4.3, we defined three main types of events, classified by proton intensity profiles, which we would like to predict by three distinct methods. These methods are (1) Type 1 alerts: geared towards fasting-rising proton events (2) Type 2 alerts: geared towards slow-rising proton events and (3) Type 3 alerts: geared towards follow-on proton events. By dividing our algorithm into three types of alerts, we can more specifically develop a prediction scheme to their distinct profiles.

The three components of this algorithm are inter-related based on common threshold values. The next three sections will discuss each algorithm independently, while a logic diagram demonstrating the organization of this algorithm as a whole can be found in Figure 6.1. The number beneath each step in the logic diagram indicates the section in which the justification for this component of the algorithm can be found.

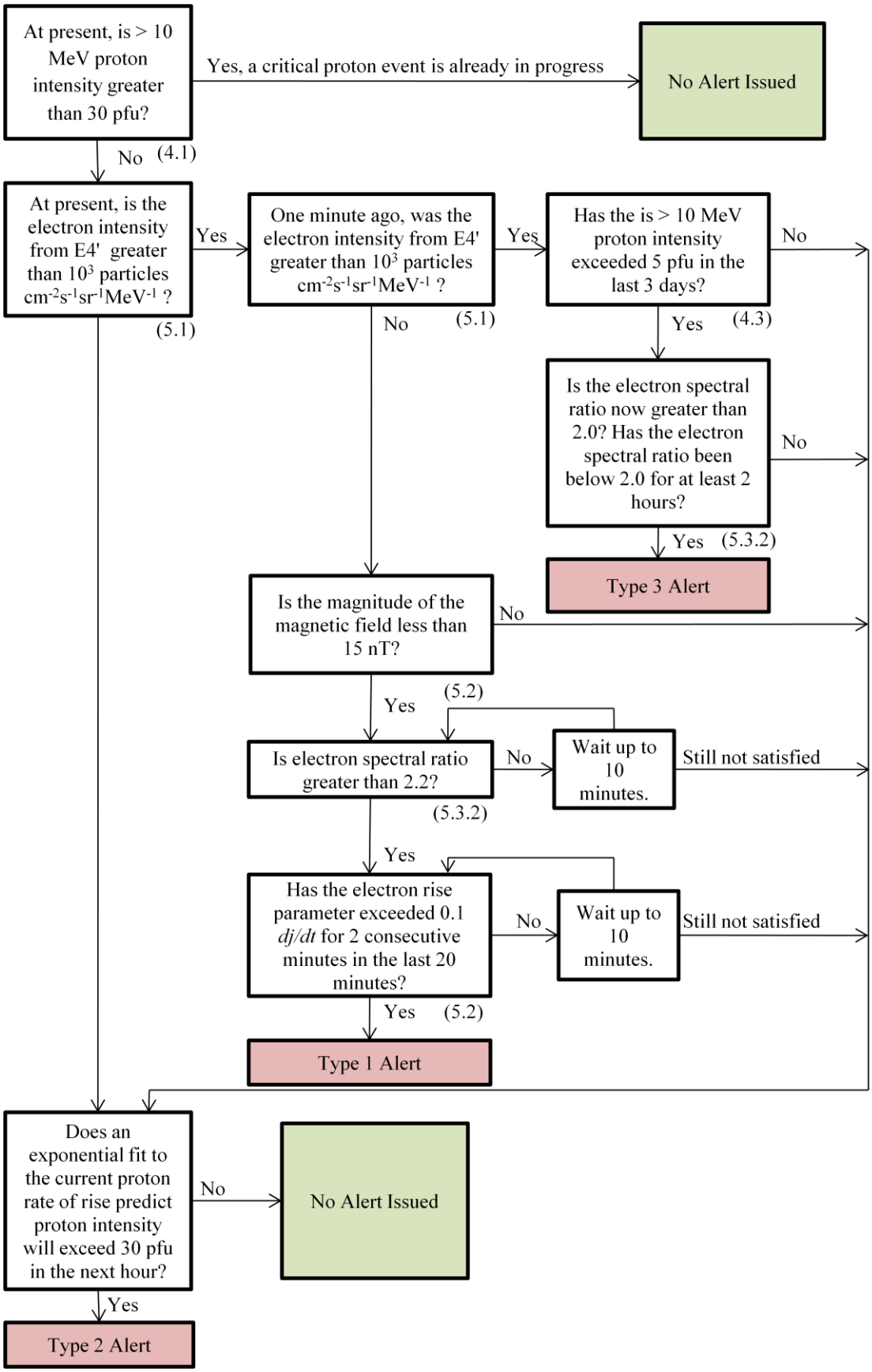
At present, is > 10 MeV proton intensity greater than 30 pfu?
Yes, a critical proton event is already in progress
No Alert Issued
No (4.1)
At present, is the electron intensity from E4' greater than 10^3 particles $cm^{-2}s^{-1}sr^{-1}MeV^{-1}$?
Yes
(5.1)
One minute ago, was the electron intensity from E4' greater than 10^3 particles $cm^{-2}s^{-1}sr^{-1}MeV^{-1}$?
Yes
No (5.1)
Has the is > 10 MeV proton intensity exceeded 5 pfu in the last 3 days?
No
Yes (4.3)
Is the electron spectral ratio now greater than 2.0? Has the electron spectral ratio been below 2.0 for at least 2 hours?
No
Yes (5.3.2)
Type 3 Alert
Is the magnitude of the magnetic field less than 15 nT?
No
(5.2)
Yes
Is electron spectral ratio greater than 2.2?
No
Wait up to 10 minutes.
Still not satisfied
(5.3.2)
Yes
Has the electron rise parameter exceeded 0.1 *dj/dt* for 2 consecutive minutes in the last 20 minutes?
No
Wait up to 10 minutes.
Still not satisfied
Yes (5.2)
Type 1 Alert
Does an exponential fit to the current proton rate of rise predict proton intensity will exceed 30 pfu in the next hour?
No
No Alert Issued
Yes
Type 2 Alert

Fig 6.1 - Logic diagram of connection between Type 1, 2, and 3 Alerts

6.1 Type 1 Alerts

The defining feature of the events predicted by Type 1 alerts is the large electron rise parameter measured at the onset of these events. This indicates that an event may be magnetically well-connected and that scatter-free propagation conditions may be present in the interplanetary medium. The distribution of the maximum electron rise parameter observed during event onset has a maximum around 0.05 $\frac{d \log (j)}{dt}$, with a tail that extends to just below 0.5 $\frac{d \log (j)}{dt}$ (Figure 6.2).

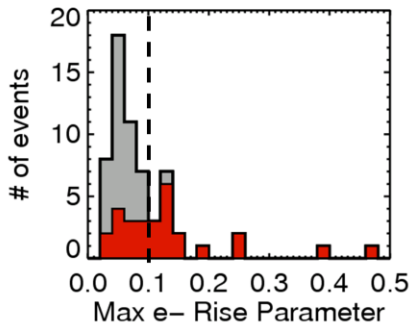

Fig 6.2 - Histogram of electron sliding rise parameter for all 61 critical events listed in Table 4.1. In red are those events with an event onset duration less than 120 minutes (immediate events). The rise parameter threshold, discussed in Section 6.1.1 criterion 3, is indicated by the dotted line. More than half of the critical events (16 out of 28) have a maximum rise parameter above 0.1 $\frac{d \log (j)}{dt}$.

6.1.1 Type 1 Alert Algorithm

A Type 1 alert is issued when the following conditions are satisfied:

(1) Differential electron intensity of EPAM channel E4' must originate below a threshold of 10^3 particles cm^{-2} MeV^{-1} sr^{-1} s^{-1}, and exceed that threshold. The crossing of this threshold indicates electron onset.

(2) Integral proton intensity of >10 MeV protons must be less than 30 pfu. This indicates that a proton event is not already in progress.

(3) The electron sliding rise parameter must be greater than 0.1 $\frac{d \log (j)}{dt}$ for two consecutive minutes in a 30 minute window, starting 20 minutes before and extending 10 minutes after the electron intensity crosses threshold. This window allows for the steepest rise of electron onset and the time at which electron intensity crosses threshold to be temporally offset

(4) The magnitude of the magnetic field |B| measured at ACE must be less than 15 nT. This indicates that it is unlikely that a steep electron rise parameter was produced by the transition of the spacecraft into a new magnetic flux tube, which can result in increased particle intensities but does not indicate the beginning of event onset.

(5) If the electron spectral ratio is less than 2.2 at the event trigger, it must exceed this ratio (soften) in the next 10 minutes, indicating an observed velocity dispersion for scatter-free propagation.

Figure 6.3 is an example of a critical event for which a Type 1 alert is issued.

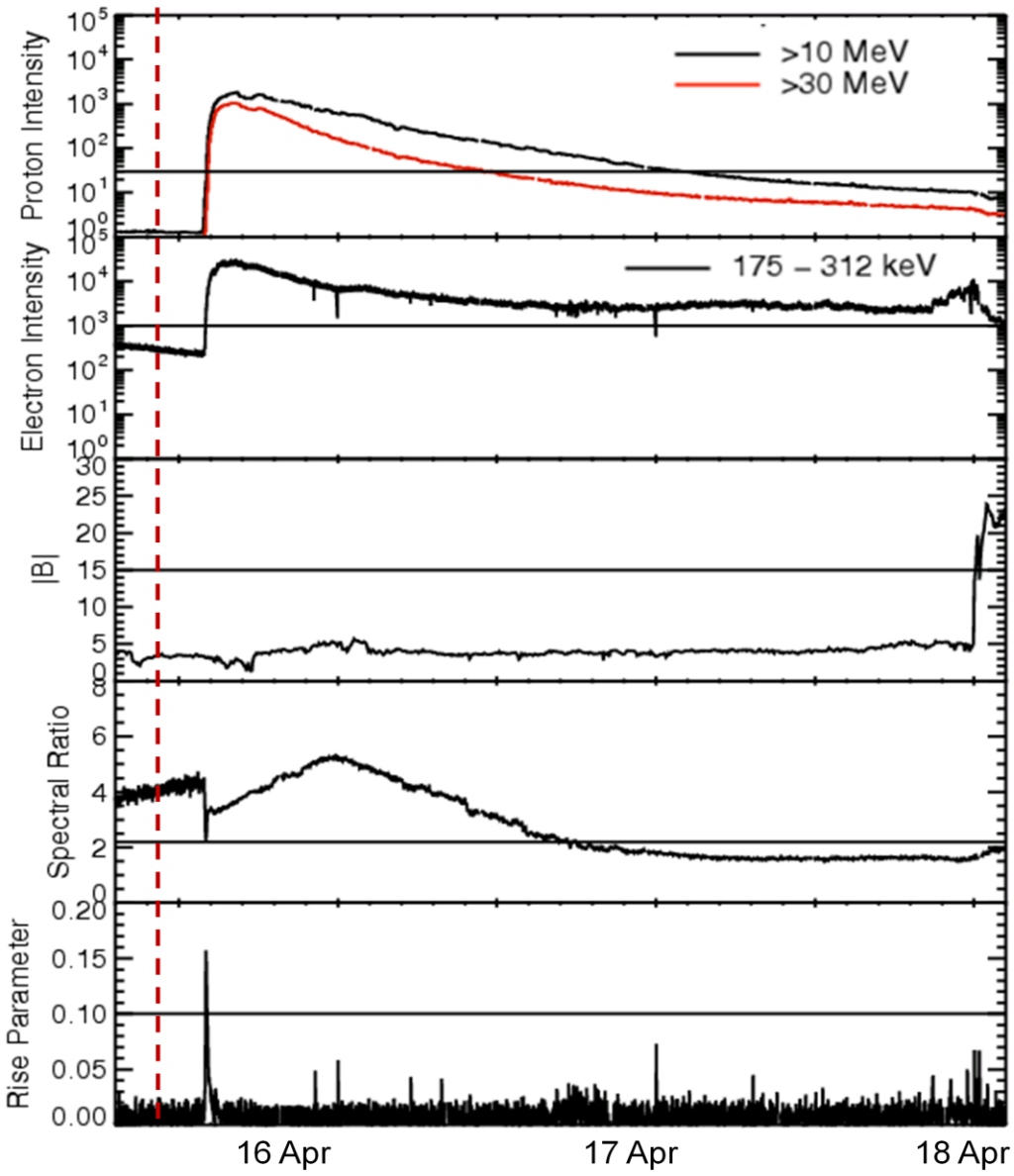

Fig 6.3 – Critical event from 15 April 2001 (DOY=105). (a) Proton intensity is below threshold at time of electron onset. Proton intensity exceeds 30 pfu at 14:15 on 15 Apr, 4 minutes after event prediction. (b) Electron intensity onsets at 14:01 on 15 April and crosses threshold at 14:11. (c) The magnitude of the interplanetary magnetic field is less than 15 nT during event onset. (d) Spectral ratio hardens at beginning of electron onset, then softens above the 2.2 threshold. (e) The electron rise parameter exceeds 0.1 $d\log(j)/dt$ during electron onset. Note the passage of a shock on 18 Apr (DOY = 108).

6.2 Type 2 Alerts

Type 2 alerts are issued base on the observation of a continued increase in proton intensity for an extended period of time before it reaches hazardous levels. In this scheme, the signature of electrons is not useful, as they have no characteristic rise over this time. Therefore, we use the rise of the protons themselves to predict their continued onset. To do so, we define the proton rise parameter, a linear fit to the slope of the proton time-intensity profile in semi-log space over 60 minutes. Assuming continued onset, this rise is propagated forward in time to predict the proton intensity one hour later, triggering a warning if the predicted intensity is > 30 pfu.

6.2.1 Type 2 Alert Algorithm

A Type 2 alert is issued when the following conditions are satisfied:

(1) Integral proton intensity of >10 MeV protons must be less than 20 pfu. This indicates that an event is not already in progress, and mitigates the problem of small fluctuation around 30 pfu causing multiple triggers, based on a linear fit to the last 60 minutes of log(j_{proton}).

(2) Predicted (+60min) Integral Proton intensity of >10 MeV protons must be greater than 30 pfu

(3) No requirements on the IMF.

Figure 6.4 is an example of a critical event for which a Type 2 alert is issued.

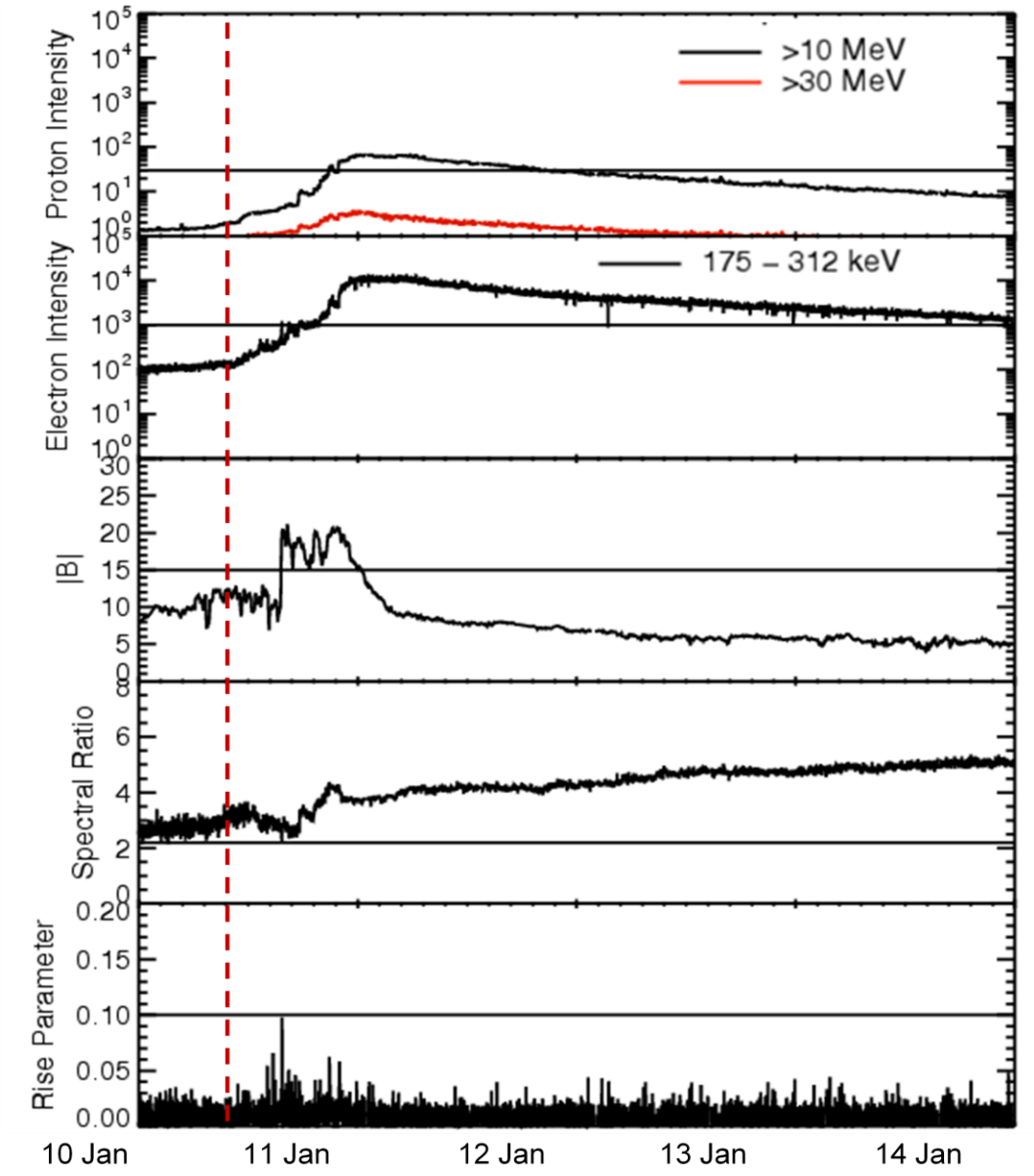

Fig 6.4 – Critical event from 10 January 2002 (DOY=10). (a) Event is predicted at 21:01. Proton intensity exceeds 30 pfu 175 minutes later. (b) Electron intensity is an irrelevant parameter in this prediction scheme. (c) No requirements are placed on the IMF for this type of event. (d) Spectral ratio is an irrelevant parameter for this prediction scheme. (e) The electron rise parameter does not exceed 0.1 *dlog(j)/dt* during electron onset.

6.3 Type 3 (Follow-On) Events

Those critical events which follow closely behind another event, are the most difficult to forecast because the interplanetary medium has been altered by the passage of the previous event and, in many cases, large electron intensities may still be present while the proton intensity has

decayed below threshold. A key assumption of this prediction scheme is that the spectral ratio of the preceding event evolves in a predictable way. Abrupt deviation from this behavior indicates the arrival of a new particle population.

Looking at the list of proton events (Table 4.1) allows us to get a rough idea of how frequently follow-on events occur. Of the 61 events listed, 7 (Events #: 8, 21, 28, 29, 37, 44, 61) of these occur within 3 days of the onset of the previous event. This is not the whole story, though since these are only the largest of the proton events. Proton intensities below our established threshold of 30 pfu can be accompanied by large electron intensities. Furthermore, near-relativistic impulsive electron events can produce large, short-term increases in the background electron intensity, obscuring the onset rise signature.

6.3.1 Type 3 Alert Algorithm

A Type 3 alert is issued when the following conditions are satisfied:

(1) Differential electron intensity of EPAM channel E4' must be elevated above the Type 1 electron intensity threshold (10^3 particles $cm^{-2}s^{-1}sr^{-1}MeV^{-1}$). This indicates that the electron onset may be obscured.

(2) Integral proton intensity of > 10 MeV protons must be less than 30 pfu. This indicates that an event is not already in progress

(3) Integral proton intensity of > 10 MeV protons must have been less than 5 pfu in the last 3 days, indicating that an event has recently occurred.

(4) The electron spectral ratio must have been below a threshold ratio of 2.0 for two hours, and then exceed this threshold, indicating the arrival of a new population of particles.

(5) No criteria are set on the IMF.

A typical critical event predicted by a Type 3 alert is shown in Figure 6.4. The initial proton onset on 2 Nov is predicted by a Type 1 alert. The secondary onset on 5 Nov is predicted by a Type 3 alert.

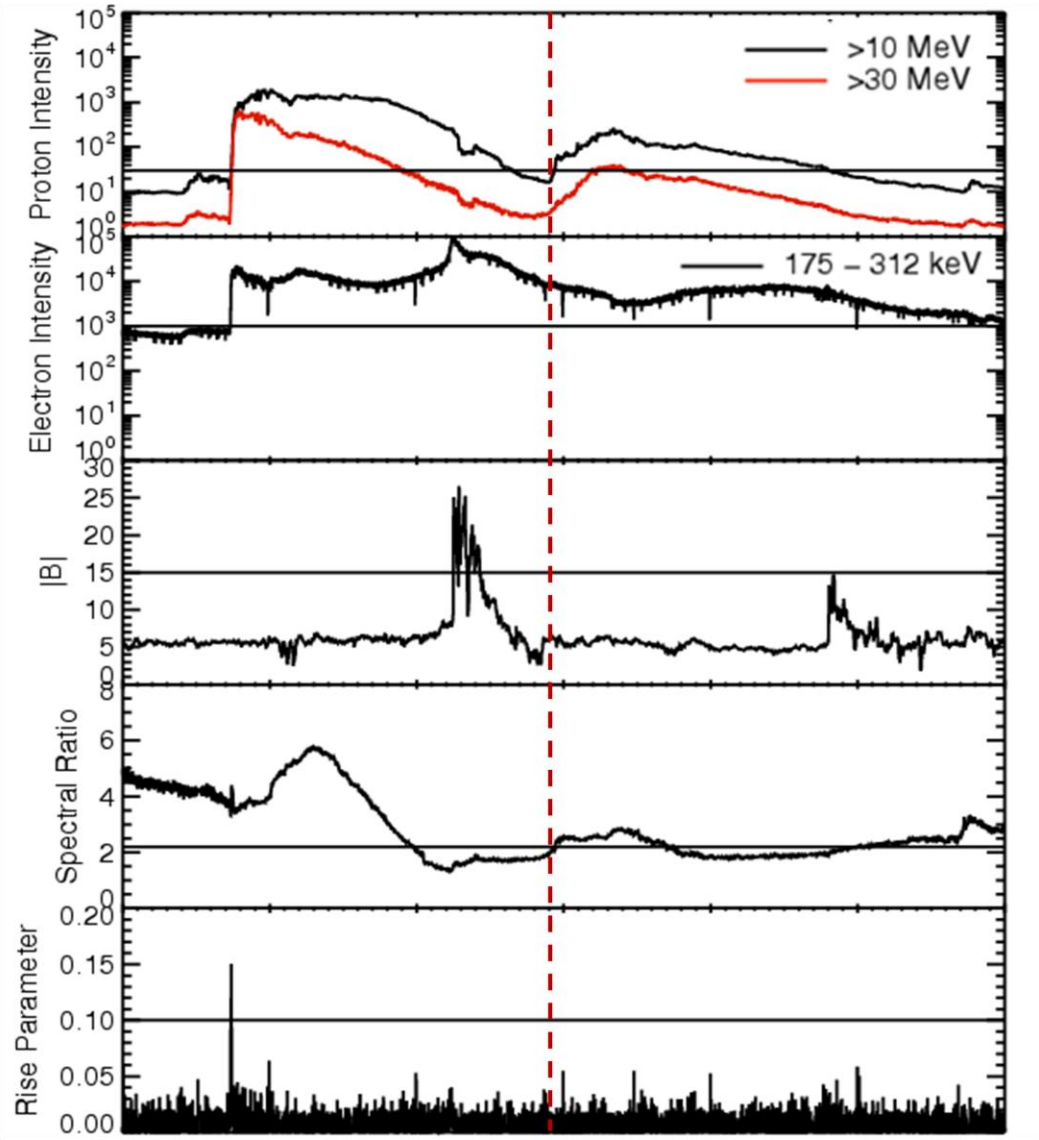

Fig 6.4 – Critical event from 5 November 2003 (DOY=309) following an event on 2 November (DOY=306) (a) Electron intensity is elevated above threshold. (b) Proton intensity from previous event has decayed below 30 pfu (c) The electron spectral ratio is below 2 for two hours, and then crosses threshold at 21:48 on 4 Nov. Protons cross threshold 45 minutes later. (d) The electron rise parameter does not exceed 0.1 *d*log*(j)/dt* during electron onset, as there is no defined electron onset for this event. (e) The IMF is not required to be quiet for this type of event.

7 Results - Analysis of Algorithm

To analyze the algorithm outlined in Section 6, we applied it to all ACE data from 1998 to 2006 and define three quantities: (1) efficiency, (2) prediction probability, and (3) median prediction time. These measures are dependent on the number of critical events in the time period in question (*CE*), the number of critical events correctly predicted by an alert (*CA*), and the number of alerts which are not followed by a critical event (*FA*).

(1) Prediction efficiency – percentage of critical events that are successfully predicted by the algorithm: $\left(\frac{CA}{CE}\right)$. The combined efficiency of these three algorithms is 96% (27 out of 28) for immediate events and 80% (49 out of 61) for all proton events.

(2) Prediction probability – percentage of events predicted by the algorithm that achieve critical events status (reach a peak proton intensity greater than 30 pfu): $\left(\frac{CA}{CA+FA}\right)$. Prediction probability allows users to make operational decisions based on certainty associated with an alert. When any of the three alerts are triggered, there is a 39% probability that it will be followed by a >10 MeV proton event which reaches 30 pfu within the next three hours. Individual prediction probabilities of each of the three alerts are discussed in subsequent sections.

(3) Median prediction time – median time from alert notice until proton intensity exceeds 30 pfu for all "Critical Events" for which alerts are issued. The median prediction time for all 49 events preceded by alerts is 38 minutes. This metric with be evaluated for each event type in the subsequent sections.

Table 7.1 summarizes the results obtained when these three combined algorithms are applied to EPAM/LEFS60 electron data from 1998-2006.

	# of Alerts Issued (A)	# of Events Correctly Predicted (CA)	# of False Alerts (FA)	% of Critical Events Predicted (CA/61)	Event Probability (CA/A)	Median Warning Time (minutes)
Type 1	26	17	9	27.9 %	65.4 %	18
Type 2	77	26	51	42.6 %	33.8 %	67
Type 3	24	6	18	9.8 %	25 %*	69
Total	127	49	78	80.3 %	38.6 %	38

7.1 Type 1 Alerts

Table 7.1 lists the 17 "Critical Events" predicted by the Type 1 alert algorithm presented in section 6.1.1.

7.1.1 Type 1 Prediction Effectiveness

This algorithm issues 26 alerts, 17 of which are followed by a critical event that reaches a maximum intensity of at least 30 pfu, yielding an prediction probability of 65%. 16 of these 17 events are immediate events, having proton onsets less than 2 hours. The median prediction time for these 17 Type 1 alerts is 18 minutes. The main determinant of the prediction time for a given event is proton onset duration (Figure 7.1).

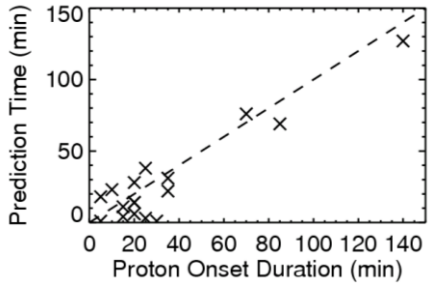

Fig 7.1 - Correlation between prediction time and proton onset duration. The dotted line indicates an event which is predicted in the same minute as when the first protons in that event are observed.

TYPE 1 ALERTS											
Event #	Year	DOY	Electron Start Date	Max Electron Intensity	Max e^- Rise Parameter	Assoc. Flare Loc.	SRP† Max	Max Proton Intensity (pfu)	>30 MeV Protons HPFU†	Proton Onset (min)	Forecast Time (min)
3	1998	126	6-May	9.21E+03	0.40	W65	N	436	Y	5	18
6	1998	318	14-Nov	1.43E+04	0.14	W90	N	218	Y	30	1
9	2000	49	18-Feb	4.53E+03	0.24	E07	N	46	N	70	76
12	2000	162	10-Jun	4.81E+03	0.12	W38	N	134	Y	20	28
15	2000	313	8-Nov	1.89E+05	0.47	W75	N	4796	Y	25	38
20	2001	105	15-Apr	2.93E+04	0.15	W85	N	1813	Y	15	4
22	2001	228	16-Aug	4.47E+04	0.13	back	N	536	Y	35	22
25	2001	308	4-Nov	7.87E+05	0.12	W18	Y	4745	Y	25	3
27	2001	360	26-Dec	1.43E+04	0.13	W54	N	1218	Y	20	6
32	2002	111	21-Apr	2.48E+04	0.24	W84	N	2093	Y	15	11
37	2002	236	24-Aug	7.44E+03	0.12	W90	N	314	Y	20	14
41	2003	299	26-Oct	1.15E+04	0.13	W38	N	417	Y	35	31
43	2003	306	2-Nov	1.11E+05	0.12	-	N	1863	Y	5	1
49	2004	263	19-Sep	4.36E+03	0.13	W58	N	75	N	140	127
50	2004	306	1-Nov	3.65E+03	0.11	back	N	129	Y	20	14
54	2005	167	16-Jun	3.95E+03	0.12	W87	N	89	Y	85	69
60	2006	347	13-Dec	8.01E+04	0.20	W23	N	1453	Y	10	23

†SRP Max: Shock-related proton maximum: event maximum > 10 MeV proton intensity occurs at the passage of shock (Yes/No)
HPFU: Human Proton Flux Units: Integral flux of >30 MeV protons reach threat levels (30 pfu) for biological systems (Yes/No)

Table 7.1 - List of Solar Particle Events predicted based on electron intensity and rise parameter (see Section 5.2).

7.1.2 Type 1 False Alerts

In the 9 years covered in this study, this algorithm incorrectly predicts the onset of a solar proton event 9 times. These "false alerts" can be classified into three main categories:

(1) Sharp electron onset, followed by gradual decay, on the time scale of days (Figure 7.2a). These triggers are usually accompanied by a delayed onset > 10 MeV protons, which do not attain the 30 pfu threshold intensity to qualify as an event. There are 4 false alerts that exhibit this behavior, with an average maximum proton intensity of 12.04 pfu.

(2) Sharp electron onset, followed by quick decay, on the time scale of hours (Figure 7.2b). These impulsive events are not accompanied by > 10 MeV protons. There are 2 false alerts that exhibit this behavior. Most impulsive electron events are avoided by setting a high enough threshold on electron intensity. "Spike" electron events have characteristically soft spectra compared to their more gradual counterparts (Haggerty & Roelof, 2009). We see a softening of the spectral ratio for these two events, which occurs 7 minutes after electrons cross threshold for the trigger on 1 May 2000 and 4 minutes after the trigger on 20 Oct 2002. Therefore, we could eliminate false triggers of this nature by waiting additional time to identify this spectral feature.

(3) Particle onset accompanies the arrival of magnetic structure (Figure 7.2c). The particle population can fluctuate immediately as the spacecraft transits into distinct flux tubes. Two false alerts, triggered by a jump in proton intensity, are followed closely by a sharp increase in the magnitude of the IMF and are identified by Cane and Richard's list of near-earth interplanetary coronal mass ejections, as having associated magnetic clouds, large coherent flux ropes with strong magnetic fields (Gosling, 1990).

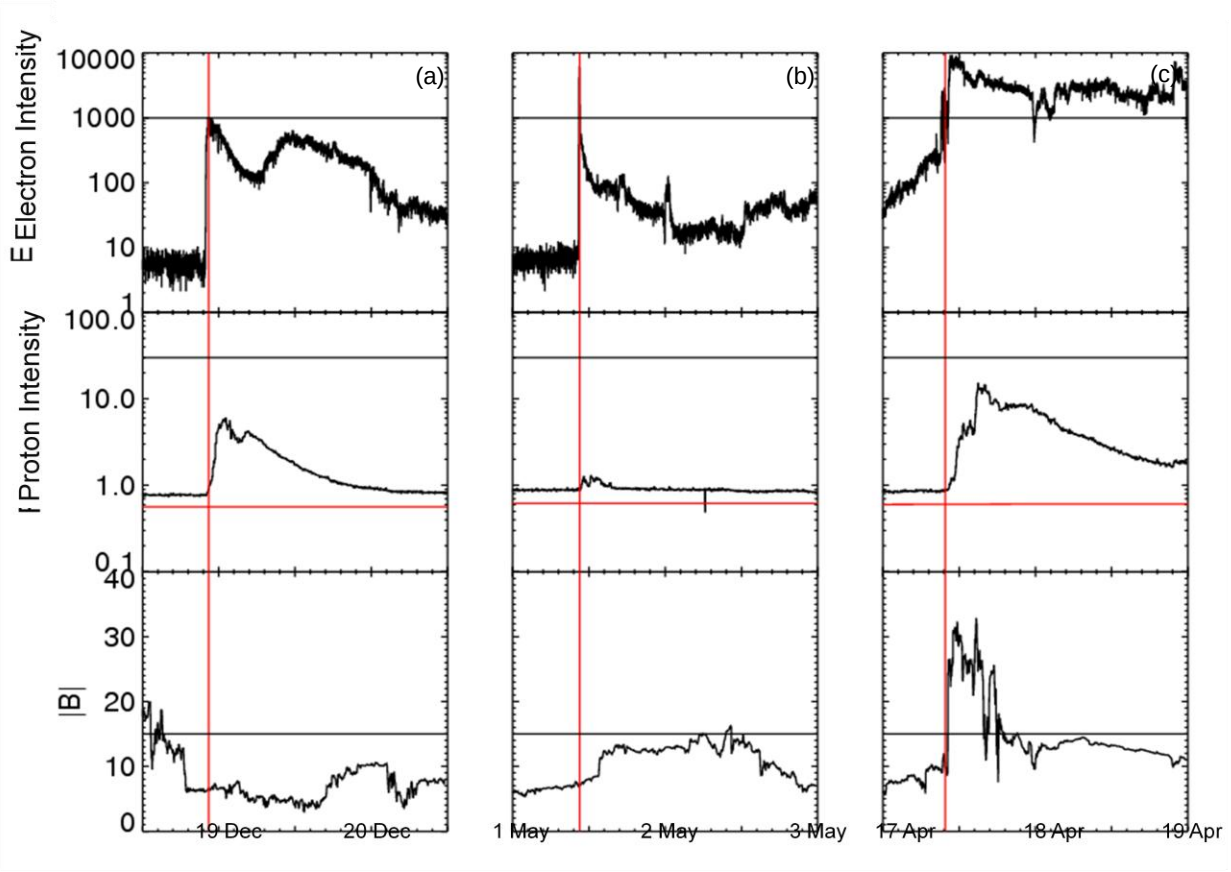

Fig 7.2 – Example "false alert" Type 1 event predictions. Vertical lines (red) indicated the time of event predictions (a) Minor solar particle event, plotted over 2 days (b) Impulsive electron events, plotted over 2 days (c) Particle enhancement related to magnetic flux , plotted over 2 days

7.1.3 Dependence of Type 1 Efficiency on Algorithm Parameters

In an attempt to optimize this prediction scheme, we compared the number of events correctly predicted by this component of the algorithm to the number of false alert warnings it generated (Figure 7.3). The set threshold of 10^3 particles $cm^{-2}s^{-1}MeV^{-1}sr^{-1}$ maximizes the number of events predicted by this algorithm, if the rise parameter threshold is held constant at 0.1 $\frac{d\log(j)}{dt}$.

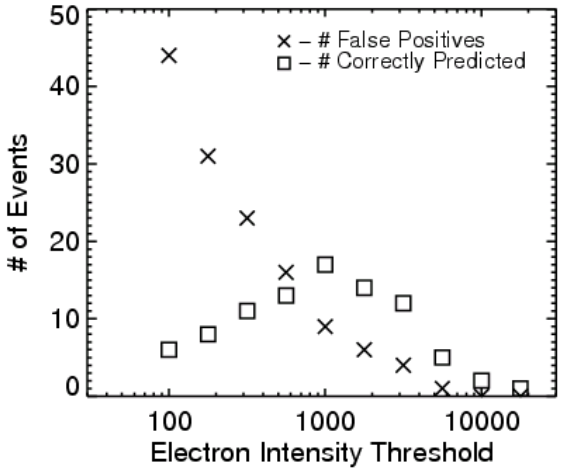

Fig 7.3 - Dependence of event prediction through electron onset on electron intensity threshold, with the rise parameter threshold fixed at 0.1 $\frac{d \log (j)}{dt}$. The current algorithm operates at the threshold of 10^3 particles $cm^{-2}s^{-1}MeV^{-1}sr^{-1}$.

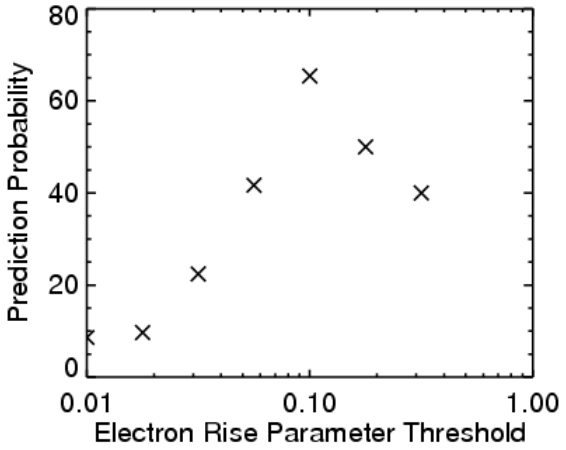

Fig 7.4 - Dependence of prediction probability through electron onset on electron rise parameter threshold, at a constant electron intensity threshold of 10^3 particles $cm^{-2}s^{-1}MeV^{-1}sr^{-1}$. The current algorithm operates at the threshold of 0.1 $\frac{d \log (j)}{dt}$.

7.2 Type 2 Alerts

Table 7.2 lists the 26 "Critical Events" predicted by the Type 2 alert algorithm presented in section 6.2.1.

7.2.1 Type 2 Forecasting Effectiveness

This algorithm issues 77 alerts, 26 of which are followed by a critical event that reaches a maximum proton intensity of at least 30 pfu, yielding a prediction probability of 34%. 7 of these 26 events are immediate events, having proton onsets less than 2 hours. The median prediction time for the critical events preceded by Type 2 alerts is 67 minutes.

TYPE 2 ALERTS								
Event #	Year	DOY	Start Date*	Proton Onset Time	Max Proton Intensity (pfu)	Proton Onset Duration (min)	Associated Active Region Long.	Forecast Time (min)
1	1998	110	20-Apr	11:04	1318	225	W90	136
2	1998	122	2-May	13:53	160	20	W15	2
4	1998	236	24-Aug	22:37	167	75	E07	25
5	1998	273	30-Sep	14:08	882	90	W81	62
8	1999	155	4-Jun	8:12	51	85	W69	35
14	2000	256	12-Sep	13:38	208	260	W09	101
16	2000	329	24-Nov	5:43	646	655	W05	165
17	2001	28	28-Jan	17:03	51	465	W59	90
18	2001	92	2-Apr	22:32	1022	55	W82	32
19	2001	100	10-Apr	16:02	229	1130	W09	72
23	2001	267	24-Sep	11:41	3705	95	E23	57
26	2001	326	22-Nov	21:02	3652	165	W34	127
28	2001	363	29-Dec	1:56	47	310	E90	93
30	2002	10	10-Jan	11:12	67	590	E limb	175
34	2002	188	7-Jul	12:32	30	410	W limb	100
35	2002	197	16-Jul	11:57	121	520	W01	95
36	2002	234	22-Aug	2:32	32	120	W62	101
38	2002	250	7-Sep	3:12	208	2115	E28	19
39	2002	313	9-Nov	15:02	428	340	W29	31
42	2003	301	28-Oct	11:31	5820	40	E08	17
45	2003	336	2-Dec	13:03	115	160	W limb	117
46	2004	102	11-Apr	5:12	33	495	W47	30
47	2004	207	25-Jul	16:17	1296	160	W33	106
51	2004	310	5-Nov	10:06	472	550	W17	53
55	2005	195	14-Jul	15:32	145	1380	W80	55
57	2005	234	22-Aug	2:17	395	1080	W60	18

Table 7.2 - List of Solar Particle Events preceded by "Type 2 alert" based on proton onset.

7.2.2 Type 2 False Alerts

This prediction technique, which utilizes a projected future protons intensity based on its current rate of rise, is predicated on the assumption that this onset will continue at pace for at least the next hour. An unfortunate feature of this prediction scheme is that sudden spikes in proton intensity can result in proton rise parameters that do not characterize the general rise of the event onset. Intensity discontinuities can occur at as the spacecraft transitions into new flux

tubes or at sector crossings, as the spacecraft crosses the interplanetary current sheet and into an IMF of opposite polarity. There are instances when the future proton intensity deviates from this projected profile. However, we have not been able to identify a real-time signature in the interplanetary plasma that would indicate the roll-off or cessation of particle onset. There are two distinct false alerts that result from this behavior:

(1) Proton intensity rolls off and plateaus below 30 pfu (Figure 7.5a). Later, proton onset may continue and cross the 30 pfu threshold. This results in multiple alerts for a single event. These false alerts occur when the time-intensity profile of the proton onset is non-linear in log-space. There are 16 events which exhibit this behavior.

(2) Proton intensity rolls off and does not cross the 30 pfu threshold, returning to background (Figure 7.5b). These profiles comprise the majority of Type 2 false alerts, occurring 35 times in the 9 years of this study.

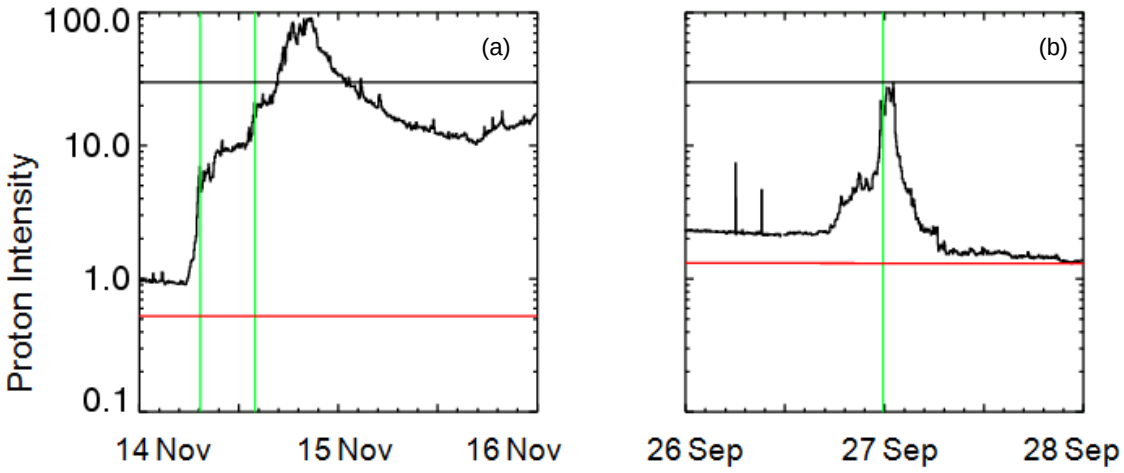

Fig 7.5 – Example "false alert" Type 2 event predictions. Vertical lines (green) indicated the time of event predictions. (a) Non-linear proton onset results in multiple event predictions, plotted over 2 days (b) Abrupt end to proton onset results in a false warning, plotted over 2 days.

7.2.3 Dependence of Type 2 Efficiency on Algorithm Parameters

Type 2 alerts are a catch-all for the other alert algorithms. As seen in Figure 6.1, when the electron signature does not result in a Type 1 or Type 3 alerts, the proton time-intensity profile may still predict the onset of a critical event. However, because this algorithm does not leverage the speed advantage of near-relativistic electrons, forecasting times for immediate events are very short. Therefore, while the number of Type 2 alerts increases as the electron intensity threshold is increased, the prediction time for these events decreases.

7.3 Type 3 Alerts

Table 7.3 lists the 6 “Critical Events” predicted by the Type 3 alert algorithm presented in section 6.3.1.

7.3.1 Type 3 Forecasting Effectiveness

This algorithm predicts 24 events, 6 of which are followed by a proton event that reaches a maximum intensity of at least 30 pfu, yielding an prediction probability of 25%. 4 of these 6 events are critical events, having proton onsets less than 2 hours. Two events predicted by this method display multiple particle injections, exceeding threshold after the third onset, causing their onset time to be extremely drawn-out. The median forecasting time of this algorithm, is 69 minutes.

TYPE 3 ALERTS									
Event #	Year	DOY	Start Date	Proton Onset Time	Max Proton Intensity (pfu) (ACE/SIS)	Proton Onset Duration (min)	Associated Active Region	Max Electron Intensity (ACE/EPAM)	Forecast Time (min)
13	2000	196	14-Jul	10:36	4382	10	W07	4.29E+05	8
21	2001	108	18-Apr	2:47	385	30	W limb	4.25E+03	94
31	2002	77	21-Mar	1:07	37	4500*	-	1.33E+05	102
44	2003	309	5-Nov	22:02	251	30	W83	1.92E+04	45
52	2005	15	15-Jan	6:57	3256	1130*	W05	1.45E+05	103
61	2006	348	14-Dec	22:47	70	5	-	8.07E+03	8
* Proton time-intensity profile exhibits multiple onsets, indicating more than one injection responsible for this event									

Table 7.3 - List of Solar Particle Events predicted based on electron spectral ratio (see Section 5.3)

7.3.2 Type 3 False Alerts

This algorithm, based on the electron spectral ratio, has the lowest prediction probability of the three methods discussed. There are three main electron profiles which produce false alert triggers for this prediction scheme:

(1) Spectral ratio correctly predicts the onset of a new particle population; however, the proton intensity of this new event does not exceed 30 pfu. There are four event predictions where this is the case (Figure 7.6a).

(2) The spectral ratio drifts over the set threshold of 2 as an event decays, indicating a softening of the spectrum as higher energies return to background more quickly than lower energies (Figure 7.6b). In most events, the spectral ratio does not begin this softening until after the electron intensity in EPAM channel E4' has decayed below 10^3 particles $cm^{-2}s^{-1}MeV^{-1}sr^{-1}$. In 8 particle events, however, the electron intensity is high enough that this threshold on the spectral ratio is crossed before electrons have decayed away. This type of false alert is most concerning because the change in spectral ratio does

not correspond to a new particle onset, but merely follows the decay of the presently pervasive population. One way that this algorithm may be improved is through the study of particle anisotropy, characterized by electron angular distribution function $j = j_0(1+\delta\cos\theta)$, where . We expect a large anisotropy measure at event onset, indicating particle streaming along field lines, followed by a smooth decay as electrons begin to back-scatter from the anti-sunward direction and the distribution function isotropizes. Including anisotropy measurements calculated from sectored EPAM data might allow for the removal of these false alerts.

(3) Impulsive burst of electrons, unaccompanied by > 10 MeV protons, are a regular feature of solar particle events (Figure 7.6c). Haggerty, Roelof, & G. Simnett (2003) identify roughly 216 "beam-like" near relativistic electron events in solar cycle 23, noting a correlation between maximum electron intensity at 17 – 312 keV and maximum proton intensity at 2-5 MeV. By setting a threshold on the electron intensity of 10^3 particles $cm^{-2}s^{-1}MeV^{-1}sr^{-1}$, we avoided triggering on these bursts. However, when the background electron intensity is already elevated, the prompt arrival of these predominately lower energy particles is identified by a discontinuity in the electron spectral ratio, resulting in a false prediction.

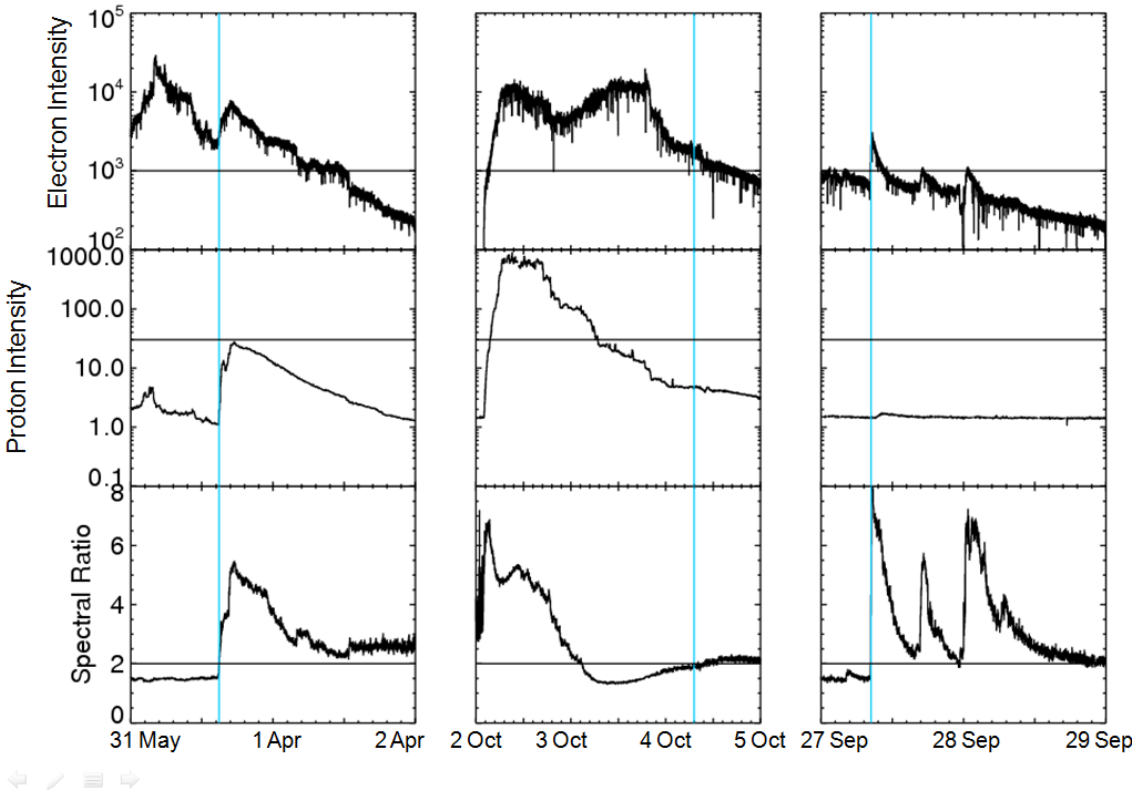

Fig 7.6 – Example "false alert" Type 3 event predictions. Vertical lines (blue) indicate the time of event predictions. (a) Spectral ratio correctly predicts particle onset, proton intensity does not exceed 30 pfu, plotted over 2 days (b) Spectral ratio crosses threshold before electron intensity has decayed below 10^3 particles $cm^{-2}s^{-1}MeV^{-1}sr^{-1}$. (c) Impulsive electron events occur while electron intensity is elevated.

7.3.3 Dependence of Type 3 Forecasting on Algorithm Parameters

In an attempt to optimize this prediction scheme, we compare the number of events correctly predicted by this component of the algorithm to the number of false alert warnings it generates (Figure 7.7). At the set threshold of 10^3 particles $cm^{-2}s^{-1}MeV^{-1}sr^{-1}$, there are still a large number of false alerts. If the threshold is increased to $10^{3.25}$ particles $cm^{-2}s^{-1}MeV^{-1}sr^{-1}$, accuracy reaches almost 50%. However, at this threshold, one critical event (18 Apr 2001) is missed because of the gap left between Type1 and Type 3 prediction. We can use the number of events predicted at an event electron threshold as a way to make a more refined prediction of the probability that a given alert will be followed by an event. We can do this because, unlike Type 1

alerts, the electron intensity at the time a Type 3 alert is issued may be anything over 10^3. By plotting the number of correctly predicted events divided by the number of type 3 alerts issued against electron intensity in the minute that an alert is issued, we see that higher electron intensity indicates that it is more likely a proton event will follow (Figure 7.8).

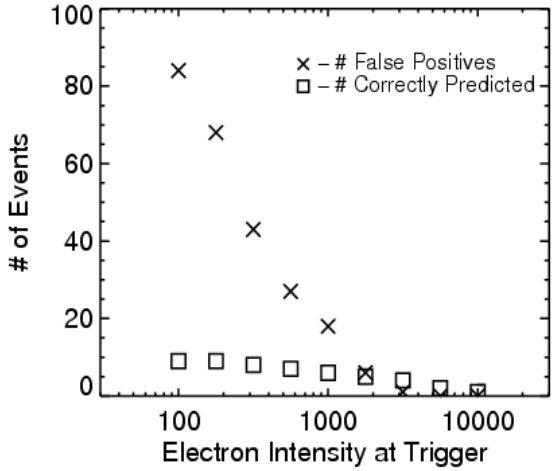

Fig 7.7 – Dependence of event prediction based on electron spectral ratio on electron intensity threshold. The current algorithm operates at the threshold of 10^3 particles $cm^{-2}s^{-1}MeV^{-1}sr^{-1}$.

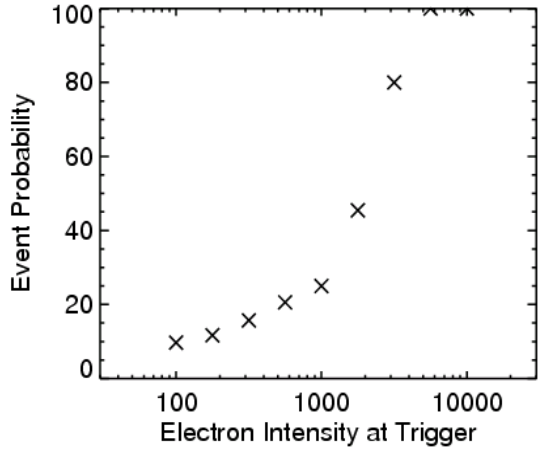

Fig 7.8– Prediction Probability of a event electron intensity measure at the minute that a Type 3 alert is issued. We see that, the higher the electron intensity at the time of the alert, the more likely there is to be a critical event following the alert. However, there are simply fewer alerts issued at these higher intensities.

7.4 Unpredicted Events

Out of the 61 "Critical Events" evaluated by in this study, 11 were not predicted by any of the three algorithms (Table 7.4). Of these 11 missed events, the highest peak proton intensity was 3140 pfu. Four of these 11 events had peak proton intensities lower than 100 pfu. There were two main causes for missed events.

(1) Too gradual of a proton onset for Type 2 alerts predicting event onset to apply. We notice that of these 11 events, all except for two had proton onset durations longer than 10 hours. Additionally, based on the flare associated active regions, only two of these 11 missed critical events originated within 20 degrees of W60. The other 9 missed critical events are poorly magnetically connected; indicating particle transport to Earth is diffusion-dominated.

(2) Electron spectral ratio of previous event did not harden enough for a Type 3 alert to be issued, contradicting the assumptions regarding the spectral ratio presented in Section 5.3.2. There are two follow-on events missed by this prediction algorithm, one of which being a critical event with a rise time of only 20 minutes. In both cases, the electron spectral ratio in the event preceding these events did not drop below expected threshold of 2.0.

MISSED EVENTS										
Event #	Year	DOY	Proton Start Date	Proton Onset Time	Max Proton Intensity (pfu) (ACE/SIS)	Max Proton Intensity (pfu) (GOES)	Proton Onset Duration (min)	Associated Active Region Long.	Max Electron Intensity (ACE/EPAM)	Event Type
7	1999	152	2-Jun	20:05	35	48	710	-	1.19E+03	2
10	2000	95	4-Apr	16:56	56	55	630	W66	5.56E+04	2
11	2000	158	6-Jun	21:33	65	84	1595	E18	5.76E+04	2
24	2001	274	1-Oct	12:57	1493	2360	20	W91	4.98E+04	3
29	2001	364	30-Dec	12:20	71	108	800	-	9.30E+03	3
33	2002	142	22-May	6:06	1150	820	970	W56	1.54E+05	2
40	2003	148	28-May	2:41	80	121	2030	W17	8.16E+04	2
48	2004	257	13-Sep	10:17	277	273	615	E42	6.63E+04	2
53	2005	133	13-May	18:26	2251	3140	670	E11	1.86E+05	2
56	2005	206	27-Jul	17:21	56	41	3335	W90	1.48E+04	2
58	2005	250	11-Sep	19:41	1513	1880	370	E89	1.45E+05	2
59	2006	339	5-Dec	13:47	2040	1980	1775	E79	2.61E+05	2

Table 7.3 - List of solar particle events not forecasted under the constraints of this algorithm.

8 Discussion

The strength of this forecasting method lays in its use real time, *in situ* particle data, while utilizing a minimal number of parameters. In total, there are four specific *in situ* measurements required by this forecasting scheme: electron intensity measurements from two near-relativistic energy channels, one high energy proton intensity measurement, and a measurement of the magnitude of the interplanetary magnetic field. Additionally, while this study was particularly geared toward developing an algorithm to predict the onset of >10 MeV protons, the thresholds are variable and may be adapted to specific space weather needs. These three measurements might theoretically be housed in one event-predicting instrument, allowing on-board activation of warning signals. Since particle anisotropy has not been investigated in this study, specific spacecraft stabilization (3-axis or spin) that would allow for the analysis of sectored data, is not required.

This prediction scheme does not estimate event intensities, nor does it predict shock associated intensity enhancements (see Cohen et al. (2001) for forecasting of ESPs at 1 AU); rather it indicates that proton intensities above a specified threshold are imminent. We find that there is not enough information in the four parameters used in this study to accurately predict maximum proton intensity. The onset profile is dictated by a combination of source region solar longitude and shock strength, and is further influenced by how these aspects evolve in time as the shock moves out to 1AU; it is difficult to separate the contributions of these two parameters to the electron rise parameter and maximum proton intensity.

By developing an algorithm which recognizes different event profiles, we are able to create a more forecasting system which is substantially grounded in the relevant physics. Type 1

and Type 3 forecasting are highly complementary, as the background electron intensity at event onset is a continuum, depending on previous electron enhancements. Type 2 forecasting, based on proton rise, most effectively predicts events which have onsets on the order of a few hours.

Appendix A. Predicting Proton Intensity from Electron Intensity and Rise Parameter

The forecasting scheme developed by Posner (2007) is attractive because of its exclusive use of *in situ* particle data. We attempted to replicate Posner's forecasting matrix using electron and proton data from ACE-EPAM and ACE-SIS. When comparing SPE forecasting models, one must be mindful that the quality of prediction schemes may vary depending on energy, influenced by variation of the characteristic knee in SEP spectrum (Kahler, 2007). To first order, the spectral index γ of an SPE associated with shock acceleration is governed by the shock compression ratio, or relationship between upstream (behind the shock) and downstream (ahead of the shock) densities, given as $r = \frac{\rho_{upstream}}{\rho_{downstream}}$. However, at some energy, the number of particles is insufficient to sustain the resonant waves necessary for particle trapping at the shock front, releasing the particles to stream out ahead of the shock, experiencing no further acceleration. A specific event profile may be highly dependent on the energy of the species under investigation.

Therefore, although the method outlined in this appendix follows Posner's procedures, we note that we are working in different energy regimes and therefore should not be surprised by less than comparable results. Table A.1 explicitly outlines the energy channels used in each study.

	Electrons	Protons
Posner	0.3 - 1.2 MeV (relativistic)	30 - 50 MeV
Kalamaroff	0.175 - 0.312 MeV (near-relativistic)	> 10 MeV

Table A.1 – Comparison of Energy channels used by Posner (2007) and by this study, from ACE-SIS and ACE-EPAM.

In this energy regime, Posner constructs a "forecasting matrix" which he uses to predict proton intensity. For an given electron intensity and electron rise parameter in a given minute, Posner's matrix predicts a proton intensity 60 minutes later (Figure A.1)

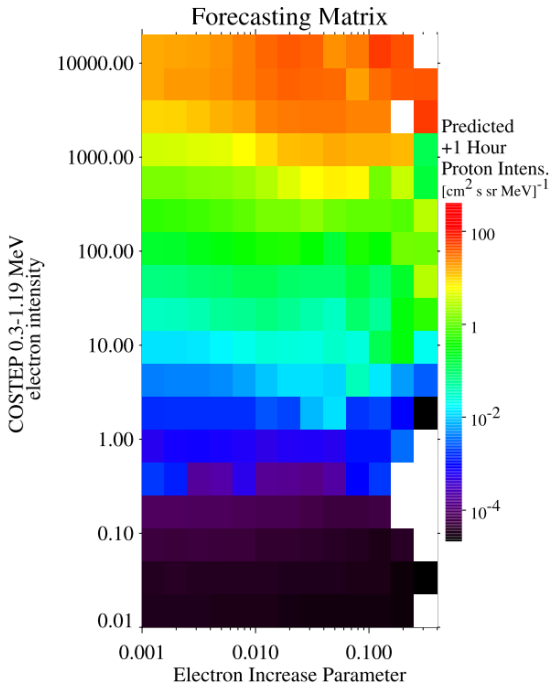

Fig A.1 – Forecasting matrix presented by (Posner, 2007). Posner's "Electron Increase Parameter" is equivalent to our electron rise parameter (presented in Section 5.2), except that he allows the fit to go back up to 60 minutes in time, selecting the maximum rise parameter in this time range. The matrix was constructed by using every minute of data from 1998 – 2002. Predicted proton intensities are determined by average upcoming (one hour later) 30-50 MeV proton intensities for each electron intensity – rise parameter combination.

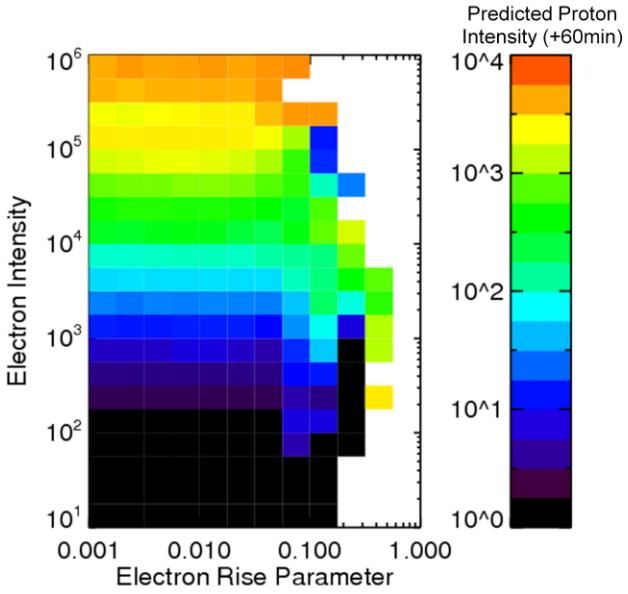

Fig A.2 – Forecasting matrix derived from ACE data based on Posner (2007) . The electron sliding rise parameter is explained in Section 5.2. . Predicted proton intensities are determined by average upcoming (one hour later) >10 MeV proton intensities for each electron intensity – rise parameter combination.

We can construct a similar forecasting matrix using ACE-EPAM rise parameter and electron intensity pair to predict proton intensity one hour later (Figure A.2). However, we want to take a closer look at each minute worth of data that contributes to the averages assigned for each box. If, for example, we look at all minutes in which the electron intensity is between 10^3

and $10^{3.5}$ and the rise parameter is between 0.1 and 0.32 $\frac{d \log (j)}{dt}$, we see that the corresponding proton intensity one hour later is broadly distributed (Figure A.3).

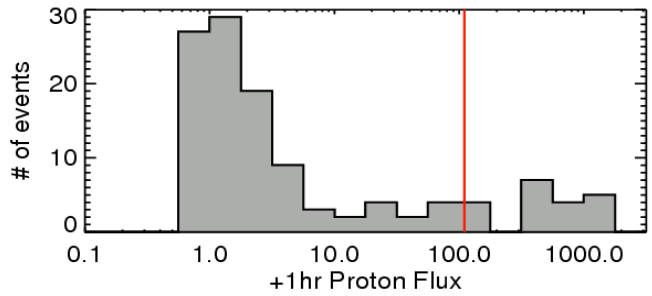

Fig A.3 – Histogram of ACE-SIS proton intensities observed one hour after a minute in which the electron intensity is between 10^3 and $10^{3.5}$ and the rise parameter is between 0.1 and 0.32. The *average* proton intensity is 110 pfu. However, we see that the distribution is far from a Gaussian distribution centered on this average.

Moving up in electron intensity, if we look at all minutes in which the electron intensity is between $10^{3.5}$ and $10^{4.0}$ and the rise parameter is between 0.1 and 0.32 $\frac{d \log (j)}{dt}$, (Figure A.4), we see that the average proton intensity is clearly higher, however, there are still many minutes in which proton intensity is not elevated above background.

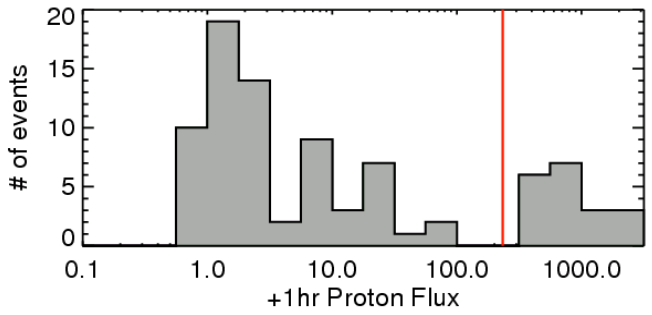

Fig A.4 – Histogram of ACE-SIS proton intensities observed one hour after a minute in which the electron intensity is between $10^{3.5}$ and $10^{4.0}$ and the rise parameter is between 0.1 and 0.32. The *average* proton intensity is 234 pfu. However, we see that the distribution is far from a Gaussian distribution centered on this average.

By looking at these distributions of +60 minute proton intensity as a function of electron intensity and electron rise parameter, we see that, although on average there is a correlation, the average proton intensity is not representative of what we might actually expect to observe.

Appendix B. Discrepancy between GOES and ACE-SIS > 10 MeV Proton Intensities

For "Critical Events" listed in Table 4.1, we notice that there are a handful of events for which ACE-SIS and GOES >10 MeV peak proton intensities are in disagreement (Figure B.1).

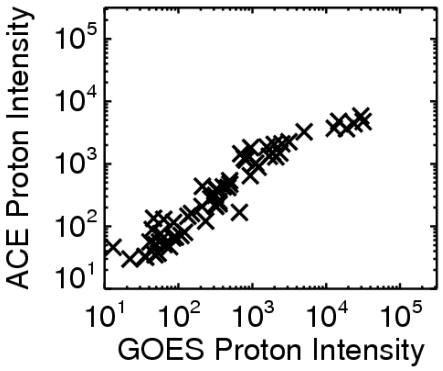

Fig B.1 – Comparison of ACE-SIS and GOES peak proton intensity for the 61 events listed in Table 4.1. We notice that some lower intensity events are in slight disagreement, while the five largest events, having GOES peak proton intensity $>10^5$ pfu are off by about an order of magnitude. The two causes of these discrepancies are discussed in the text.

One cause of inconsistencies between these two measurements is missing data from ACE-SIS. For four events, SIS >10 MeV proton intensity is temporally incomplete. While the initial proton onset is recorded, any shock-related enhancement that may occur later in the event is missed, causing the peak proton intensity to be characteristically low. These events are marked by (*) in Table 4.1

The second cause of inconsistencies, found in the most intense proton events, is the saturation of SIS >10 MeV proton channel. This saturation threshold is dependent on the amount of livetime available to this channel, which sets a maximum count rate. As particle intensities increase, the pulse heights of high Z particles will take longer to resolve, resulting in less livetime available for proton resolution. Therefore, in events where saturation occurs, SIS does not observe shock associated enhancements above this plateau, which can result in order of magnitude discrepancies (Figure B.2). Events which exhibit this discrepancy are marked by (**) in Table 4.2.

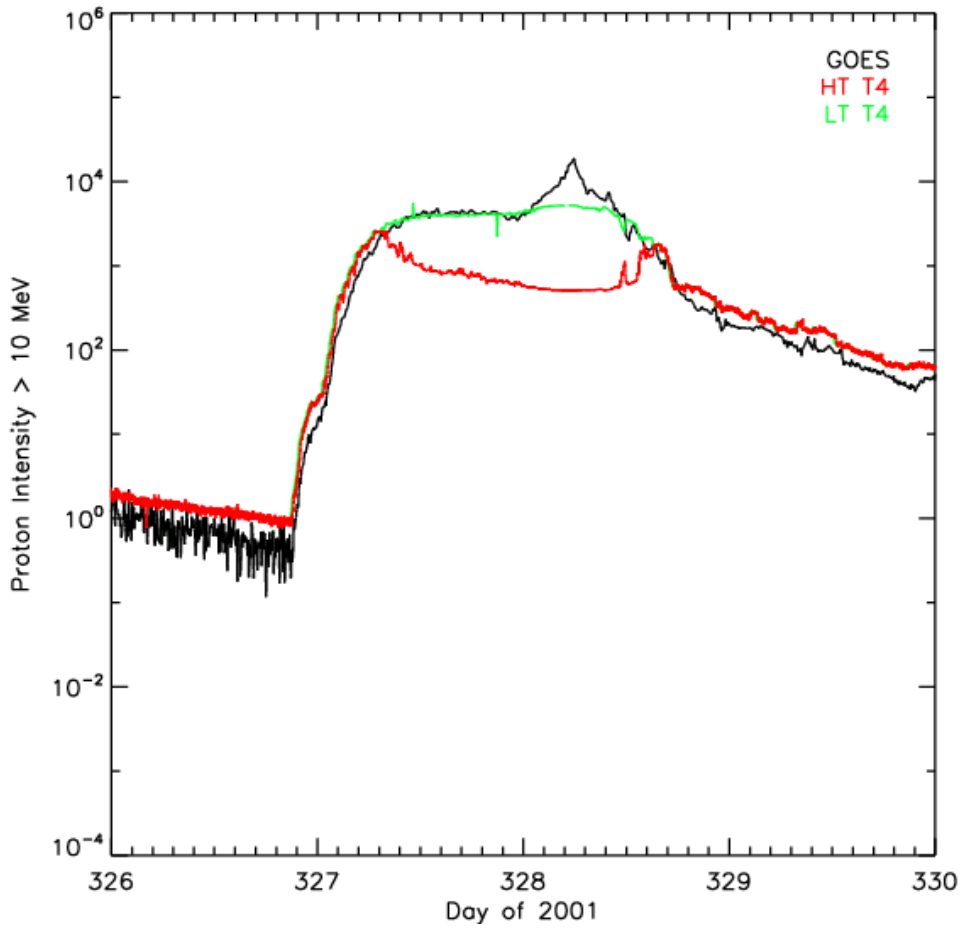

Fig B.2 – Example of a critical event from 23 Nov 2001 showing the discrepancy between GOES >10 MeV proton intensity (black) and ACE/SIS low-time resolution (green) and high-time resolution (red). ACE/SIS does not observe the shock associated particles which arrive at Earth just over a day after event onset, underestimating the peak event intensity by almost an order of magnitude.

These two inconsistencies mean that for 9 of "Critical Events" Listed in Table 4.1, ACE-SIS does not observe the shock associated enhancement of >10 MeV particles which would produce the peak intensity of the event. However, as discussed in Section 4, there are 14 critical events in which SIS does observe shock-related peak proton intensity. Therefore, to be consistent, we choose to use the GOES peak proton intensities for the events listed in Table 4.1 when evaluating the correlation of peak proton intensity to other event parameters. However, the algorithm discussed in Section 6 was applied to ACE-SIS proton data so that accurate timing could be maintained.

Appendix C. dE/dx vs. E Technique for Charged Particle Identification

The dE/dx vs. E technique uses multiple layers of silicon detectors to determine particle mass, yielding unambiguous isotopic identification. The incident particle passes through a thin silicon detector of a known thickness *L*, depositing some amount of energy, Δ*E*, and emerges with a decreased kinetic energy *E'* (Figure C.1). Using a hodoscope to trace the path of charged particles, the angle of incidence, θ, of the particle, the path length through the first detector can be determined.

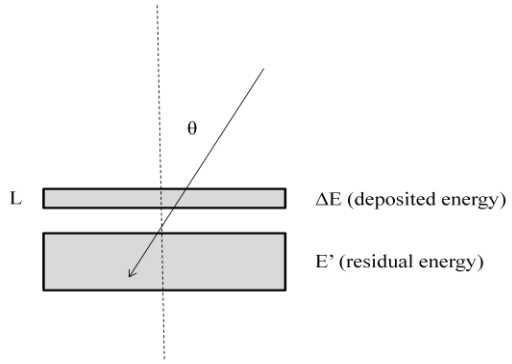

Fig C.1 – Depiction of dE/dx – E technique for charged particle identification. Particle trajectory is indicated by the arrow. While only one silicon detector of thickness *L*, is shown, the particle may also pass through more than one layer before finally depositing all of its energy.

Plotting *E'* vs. Δ*E*, particles will lie along hyperbolas of constant Z^2/M (Figure C.2). SIS uses this technique to separate particle species.

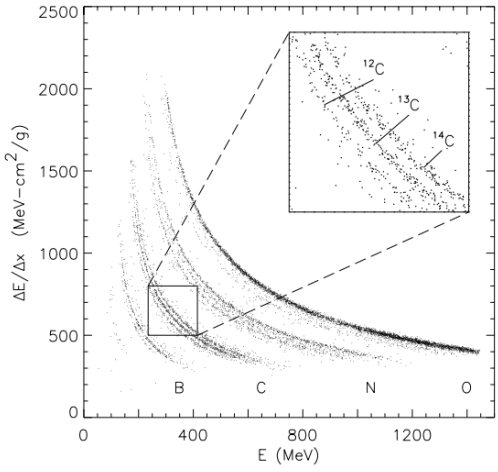

Fig C.2 – Depiction of parabolas of constant Z^2/M for dE/dx v. E. Figure from Stone et al. (1998)

Appendix D. Determining LEFS60 contamination based on Deflected Electron Data

To establish what portion of the particle signature in the electron channels on LEFS60 detector on EPAM is uncontaminated by protons which leak through the Parlyene foil in front of the detector, meant to absorbs ions below 350 keV, we compare the electron intensity from LEFS60 with the electron intensity from the deflected electron channels. The electrons measured in the deflected electron channels enter through the LEMS30 aperture, which has 51° look angle, oriented 30° degrees from the spacecraft spin axis. Using a magnet, these electrons are deflected into the back of the CA60 telescope, making these channels generally unsusceptible to ion contamination (Figure D.1). This detector has a geometry factor of 0.14 cm^2 sr, less than half of that of LEFS60 (0.397 cm^2 sr).

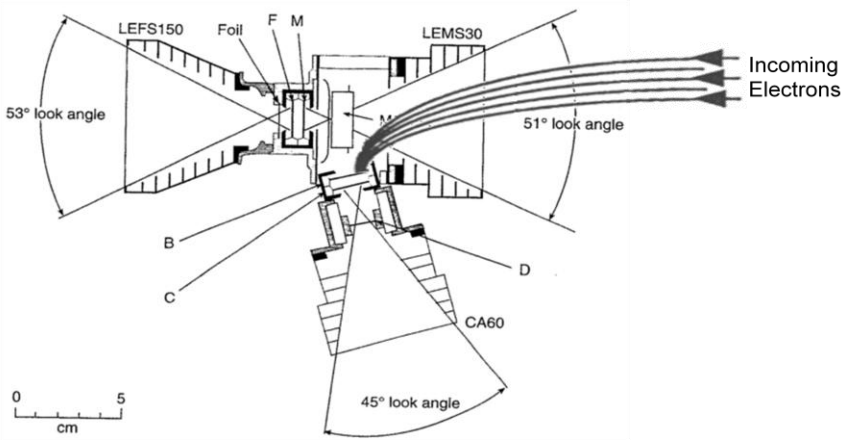

Fig D.1 – Diagram of the trajectory of the deflected electrons as they enter LEMS30 and are magnetically deflected into the back of the CA60 telescope.

Table D.1 provides a list of the energy passbands available for the deflected electrons. They are nearly identical those provided by LEFS60 (see Table 3.1).

Energy Channel	Passband (MeV)	Species
DE1	0.038-0.053	electrons
DE2	0.053-0.103	electrons
DE3	0.103-0.175	electrons
DE4	0.175-0.315	electrons

Table D.1 – Energy channels and passbands for the deflected electrons measured on ACE/EPAM

By comparing the electron intensity measured in E4' in LEFS60 to that measured in DE4, we see that these are, at times, in good agreement. Figure D.2 shows an example of a critical event from 20 April 1998 in which the intensities from these two detectors exhibit a roughly constant relationship. The electron intensity measure by LEFS60 is approximated a factor of $10^{0.2}$ lower than the deflected electrons. In this case, the electrons measured in LEFS60 are pure electrons, uncontaminated by ions.

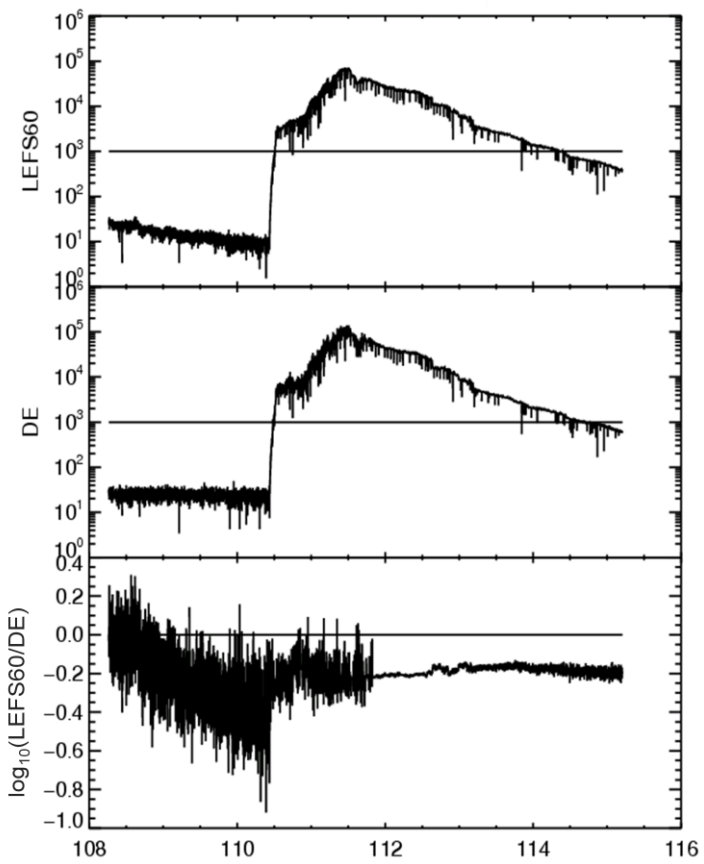

Fig D.2 – This event (critical event #1 in Table 4.1) demonstrates a time period during which the LEFS60 E4' channel is uncorrupted by ions. We see that the LEFS60 intensity is characteristically lower than the deflected electrons intensity by a factor of $10^{0.2}$.

Figure D.3 provides an example of a critical event in which the electron intensities of these two detectors are similar at event onset on 30 Sep 1998 (DOY 273), but diverge about one day later when low energy protons contaminate the E4' channel on LEFS60.

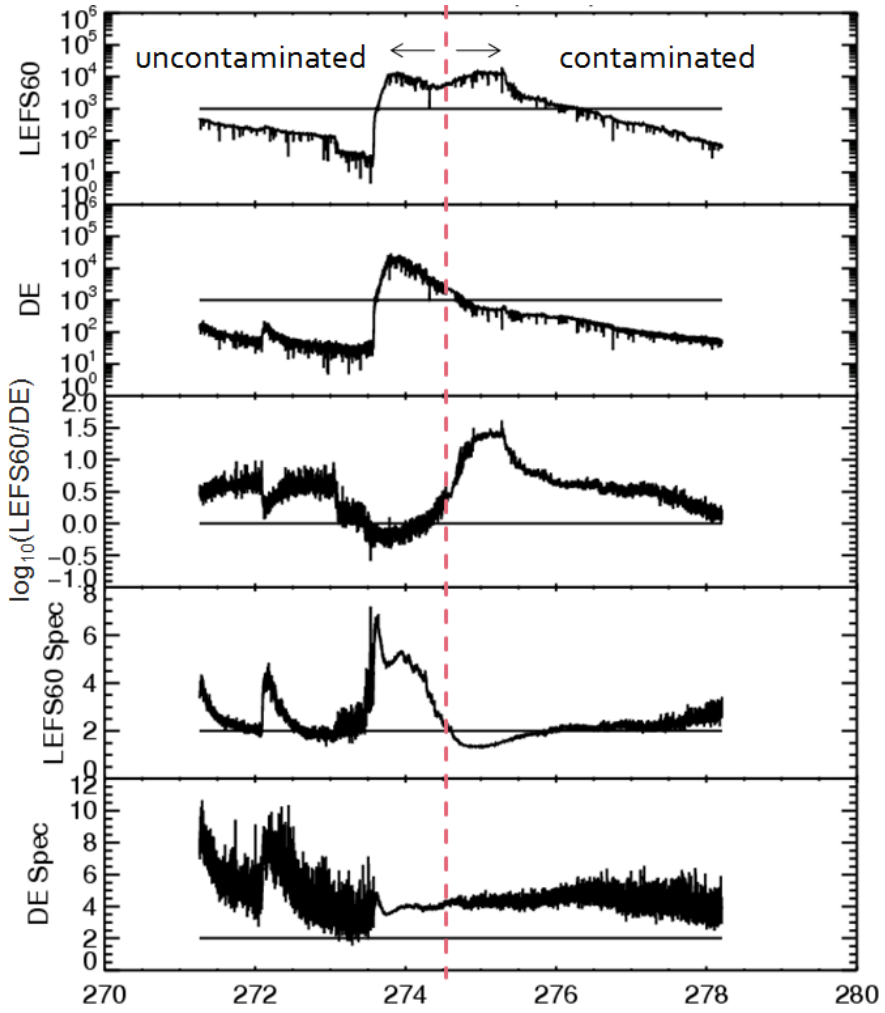

Fig D.3 – This event (critical event #5 in Table 4.1) demonstrates a time period during which the LEFS60 E4' channel is uncorrupted by ions. After approximately 1200 on 1 Oct (DOY 274), the LEFS60 electron channels become contaminated and do not accurately reflect the observed deflected electron intensities.

It is important to note how this contamination of the electron channel affects the spectral ratio from LEFS60. The observed transition of the electron spectral ratio from approximate 4.0 to less than 2.0 is not caused by a change the electron spectrum, but rather, by the corruption of the LEFS60 energy channels by protons. Since the onset phase of an event appears unaffected by the contamination of LEF60 data by ions, Type 1 alerts, in which the onset of an event is identified by electron rise parameter and intensity, should remain effective. However, since the decay phase of some events are clearly inaccurately reflected by LEFS60 data, Type 3 alerts, which

rely on the characteristic time-evolution of the spectral ration discussed in Section 5.3 to identify follow-on event onset, will be ineffective.

When we apply three algorithms outlines in Section 6 to deflected electron data from 1998-2006, with the electron threshold shifted to $10^{3.2}$ and the rise parameter threshold shifted to $10^{-0.9}$ to account for the characteristic intensity difference between LEFS60 and the deflected electrons, a total of 111 alerts are issued, successfully predicting 47 events. These results are summarized in Table D.2.

	# of Alerts Issued (A)	# of Events Correctly Predicted (CA)	# of False Alerts (FA)	% of Critical Events Predicted (CA/61)	Event Probability (CA/A)
Type 1	31	17	14	27.9 %	54.8 %
Type 2	80	30	50	49.2 %	37.5 %
Type 3	0	0	0	0 %	-
Total	111	47	64	77.0 %	42.3 %

Table D.2 – Tabulation of results achieved when algorithm is applied to the deflected electron data from 1998-2006.

The algorithm issues 0 Type 3 alerts when applied to the deflected electron data because the spectral signature produced in the LEFS60 electron intensities as an artifact of proton contamination is so longer present. Type 2 alerts are affected by the use of deflected electron data rather than LEFS60 electron intensities because they rely solely on the proton signature. Type 1 alerts issue an equal number (17) of correct event predictions for both data sets. There are, however, seven more false alerts issued when the algorithm is applied to the deflected electron data compared to the LEFS60 data set. These false alerts which are triggered in deflected electron data but not by LEFS60 data occur when the LEFS60 electron intensities are obscured by a high background of proton contamination, as shown in Figure D.4.

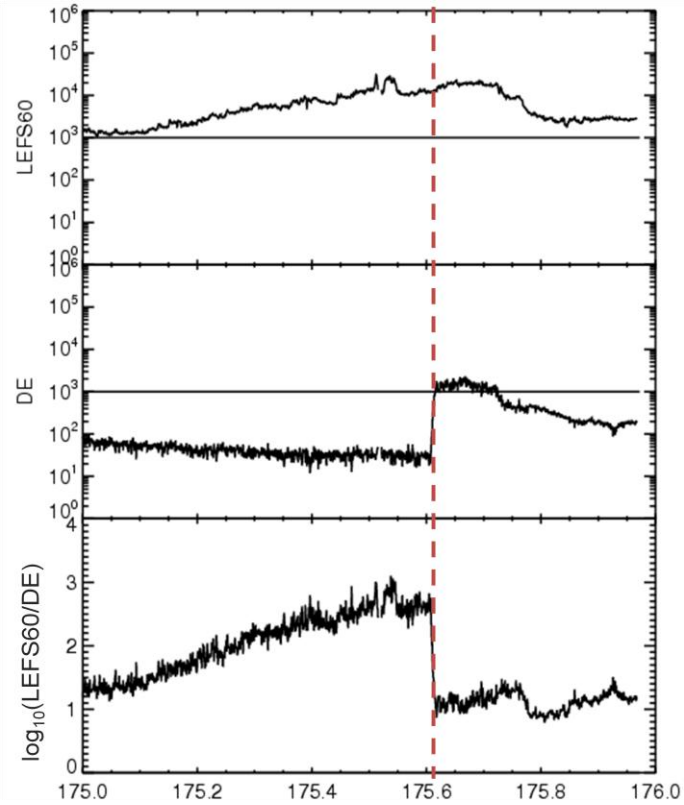

Fig D.4 – Comparison electron time-intensity during a false alert measured in the highest energy channel E4' and DE4 of LEFS60 and deflected electrons, respectively. We see that the electron signature in LEFS60 is obscured by proton contamination, while the deflected electron triggers a Type 1 alert, at the time indicated by the dotted red line, which is not followed by a critical event.

Based on this comparison of LEFS60 and deflected electron data, we conclude that the deflected electron count rates should be used in predicting solar proton events as they are simply a cleaner data product. Both Type 1 and Type 2 alert algorithms remain effective, though required adjusting based on relatively high intensities measured in the deflected electrons compared to LEFS60. The Type 3 alert algorithm is ineffective on this data set and a different mechanism would need to be developed in order to predict follow-on events.

Appendix E. Discussion of Solar Wind (SWEPAM) Data for Event Forecasting

As part of this study, we looked for identifying characteristics of particle onset in SWEPAM solar wind data, including proton density, temperature, and solar wind speed. Solar energetic particles must propagate through the solar wind in transit to 1AU, and are therefore good probes of local solar wind conditions. Solar wind speed and density can affect CME propagation and therefore shape the time-intensity profiles of these events.

However, we are interested in predicting the *onset* of particle events. Although, the solar wind exhibits characteristic behavior (discontinuous increase in proton speed, temperature, and density) at shocks, these signatures are not observed until after particle onset. Additionally, solar energetic particles may propagate into any variety of conditions in the interplanetary medium. While these conditions affect the particle's mean free path, influencing the amount of time required to travel to 1 AU, there is no characteristic signature in the solar wind which precedes particle onset. Therefore, we have no used solar wind parameters as a part of our prediction algorithm.

References

Cane, H. V., McGuire, R. E., & Von Rosenvinge, T. T. (1986). Two classes of solar energetic particle events associated with impulsive and long-duration soft X-ray flares. *Astrophys. J., 301*, 448–459.

Cane, H. V., Reames, D. V., & Von Rosenvinge, T. T. (1988). The role of interplanetary shocks in the longitude distribution of solar energetic particles. *J. Geophys. Res, 93*(A9), 9555–9567. American Geophysical Union. doi: 10.1086/592996.

Cohen, C. M. S. (2006). Observations of energetic storm particles: An overview. *Geophys. Monogr. AGU, 165*, 275. AGU AMERICAN GEOPHYSICAL UNION.

Cohen, C. M. S., Mewaldt, R. A., & Cummings, A. C. (2001). Forecasting the arrival of shock-accelerated solar energetic particles at Earth. *J. Geophys. Res, 106*(A10), 979-983.

Cohen, C. M. S., Mewaldt, R. A., Leske, R. A., Cummings, A. C., Stone, E. C., Wiedenbeck, M. E., et al. (1999). New observations of heavy-ion-rich solar particle events from ACE. *Geophys. Res. Lett., 26*(17), 2697. doi: 10.1029/1999GL900560.

Gold, R. E., Krimigis, S. M., Hawkins, S. E., Haggerty, D. K., Lohr, D. A., Fiore, E., et al. (1998). Electron, Proton, and Alpha Monitor on the Advanced Composition Explorer Spacecraft.pdf. *Space Sci. Rev., 86*, 541-562.

Gopalswamy, N., Yashiro, S., Krucker, S., Stenborg, G., & Howard, R. A. (2004). Intensity variation of large solar energetic particle events associated with coronal mass ejections. *J. Geophys. Res, 109*(A12), 105. American Geophysical Union.

Gosling, J. T. (1990). Coronal mass ejections and magnetic flux ropes in interplanetary space, *58*, 343-364. American Geophysical Union.

Haggerty, D. K., & Roelof, E. C. (2009). Probing SEP acceleration processes with near-relativistic electrons. *AIP Conf. Proc* (Vol. 1183, p. 3–10).

Haggerty, D. K., Roelof, E. C., & Simnett, G. (2003). Escaping near-relativistic electron beams from the solar corona. *Adv. Space Res., 32*(12), 2673-2678. doi: 10.1016/S0273-1177(03)00929-3.

Hollebeke, M. A. I. van, Ma Sung, L. S., & McDonald, F. B. (1975). The variation of solar proton energy spectra and size distribution with heliolongitude. *Sol. Phys., 41*(1), 189–223. Springer.

Iucci, N., Levitin, A. E., Belov, A. V., Eroshenko, E. A., Ptitsyna, N. G., Villoresi, G., et al. (2005). Space weather conditions and spacecraft anomalies in different orbits. *Adv. Space Res., 3*(1), 1-16. doi: 10.1029/2003SW000056.

Kahler, S. W., Cliver, E. W., & Ling, A. G. (2007). Validating the Proton Prediction System (PPS). *Journal of atmospheric and solar-terrestrial physics*. Air Force Research Lab Hanscom AFB MA Space Vehicles Directorate.

Laurenza, M., Cliver, E. W., Hewitt, J., Storini, M., Ling, A. G., Balch, C. C., et al. (2009). A technique for short-term warning of solar energetic particle events based on flare location, flare size, and evidence of particle escape. *Adv. Space Res.*, *7*(4), 1-18. doi: 10.1029/2007SW000379.

Li, G., Zank, G. P., & Rice, W. K. M. (2005). Acceleration and transport of heavy ions at coronal mass ejection-driven shocks. *J. Geophys. Res*, *110*, A06104. doi: 10.1029/2004JA010600.

McComas, D. J., Bame, S. J., Barker, P., Feldman, W. C., Phillips, J. L., Riley, P., et al. (1998). Solar wind electron proton alpha monitor (SWEPAM) for the Advanced Composition Explorer. *Space Sci. Rev.*, *86*(1), 563–612. Springer.

Mertens, C. J., Kress, B. T., Wiltberger, M., Blattnig, S. R., Slaba, T. S., Solomon, S. C., et al. (2010). Geomagnetic influence on aircraft radiation exposure during a solar energetic particle event in October 2003. *Adv. Space Res.*, *8*(3). doi: 10.1029/2009SW000487.

Mewaldt, R. A., Cohen, C. M. S., Haggerty, D. K., Mason, G. M., Looper, M. L., Rosenvinge, T. T. von, et al. (2007). Radiation risks from large solar energetic particle events. *AIP Conf. Proc*, 277-282. Aip. doi: 10.1063/1.2778975.

Núñez, M. (2007). Predicting Solar Energetic Proton Events (E > 10 MeV). *Adv. Space Res.*, *23*(December).

Parker, E. N. (1965). Dynamical theory of the solar wind. *Space Sci. Rev.*, *4*(5), 666–708. Springer.

Poppe, B. (2000). New scales help public, technicians understand space weather. *EOS Transactions*, *81*, 322–322.

Posner, A. (2007). Up to 1-hour forecasting of radiation hazards from solar energetic ion events with relativistic electrons. *Adv. Space Res.*, *5*(5), 1-28. doi: 10.1029/2006SW000268.

Reames, D. V. (2001). Energetic particle composition. *AIP Conf. Proc*, 153-164. Aip. doi: 10.1063/1.1433994.

Reames, D. V., Barbier, L. M., & Ng, C. K. (1996). The Spatial Distribution of Particles Accelerated by Coronal Mass Ejection–driven Shocks. *Astrophys. J.*, *466*, 473.

Smith, C. W., L'Heureux, J., Ness, N. F., Acuña, M. H., Burlaga, L. F., & Scheifele, J. (1998). The ACE magnetic fields experiment. *Space Sci. Rev.*, *86*(1), 613–632. Springer.

Speich, D., & Poppe, B. (2000). Spacecraft Anomalies. *Space Environ.*, *16*.

Stone, E. C., Cohen, C. M. S., Cook, W. R., Cummings, A. C., Gauld, B., Kecman, B., et al. (1998). The solar isotope spectrometer for the Advanced Composition Explorer. *Space Sci. Rev.*, *86*(1), 357–408. Springer.

Stone, E. C., Frandsen, A. M., Mewaldt, R. A., Christian, E. R., Margolies, D., Ormes, J. F., et al. (1998). The Advanced Composition Explorer. *Space Sci. Rev.*, *86*(1), 1–22. Springer.

Townsend, L. W. (2005). Implications of the space radiation environment for human exploration in deep space. *Radiat. Prot. Dosim.*, *115*(1-4), 44-50.